Inorg. Chem. **2006**, *45*, 9346–9366

Solid-State Coordination Chemistry of the Cu/Triazolate/X System ($X = F^-$, Cl^-, Br^-, I^-, OH^-, and SO_4^{2-})

Wayne Ouellette,[†] Andrey V. Prosvirin,[‡] Vincent Chieffo,[†] Kim R. Dunbar,*[,‡] Bruce Hudson,[†] and Jon Zubieta*[,†]

Department of Chemistry, Syracuse University, Syracuse, New York 13244, and Department of Chemistry, Texas A&M University, College Station, Texas 77842

Received June 19, 2006

Hydrothermal reactions of 1,2,4-triazole with the appropriate copper salt have provided eight structurally unique members of the Cu/triazolate/X system, with $X = F^-$, Cl^-, Br^-, I^-, OH^-, and SO_4^{2-}. The anionic components X of $[Cu_3(trz)_4(H_2O)_3]F_2$ (**1**) and $[Cu_6(trz)_4Br]Cu_4Br_4(OH)$ (**4**) do not participate in the framework connectivity, acting as isolated charge-compensating counterions. In contrast, the anionic subunits X of $[Cu^{II}Cu^{I}(trz)Cl_2]$ (**2**), $[Cu_6(trz)_4Br_2]$ (**3**), $[Cu^{II}Cu^{I}(trz)Br_2]$ (**5**), $[Cu_3(trz)I_2]$ (**6**), $[Cu_6^{II}Cu_2^{I}(trz)_6(SO_4)_3(OH)_2(H_2O)]$ (**8**), and $[Cu_4(trz)_3]OH\cdot 7.5H_2O$ (**9**·$7.5H_2O$) are intimately involved in the three-dimensional connectivities. The structure of $[Cu^{II}Cu^{I}(trz)_2][Cu_3^{I}I_4]$ (**7**) is constructed from two independent substructures: a three-dimensional cationic $\{Cu_2(trz)_2\}_n^{n+}$ component and $\{Cu_3I_4\}_n^{n-}$ chains. Curiously, four of the structures are mixed-valence Cu^{I}/Cu^{II} materials: **2**, **5**, **7**, and **8**. The only Cu^{II} species is **1**, while **3**, **4**, **6**, and **9**·$7.5H_2O$ exhibit exclusively Cu^{I} sites. The magnetic properties of the Cu^{II} species **1** and of the mixed-valence materials **5**, **7**, **8**, and the previously reported $[Cu_3(trz)_3OH][Cu_2Br_4]$ have been studied. The temperature-dependent magnetic susceptibility of **1** conforms to a simple isotropic model above 13 K, while below this temperature, there is weak ferromagnetic ordering due to spin canting of the antiferromagnetically coupled trimer units. Compounds **5** and **7** exhibit magnetic properties consistent with a one-dimensional chain model. The magnetic data for **8** were fit over the temperature range 2–300 K using the molecular field approximation with $J = 204$ cm^{-1}, $g = 2.25$, and $zJ' = -38$ cm^{-1}. The magnetic properties of $[Cu_3(trz)_3OH][Cu_2Br_4]$ are similar to those of **8**, as anticipated from the presence of similar triangular $\{Cu_3(trz)_3(\mu^3\text{-}OH)\}^{2+}$ building blocks. The Cu^{I} species **3**, **4**, **6**, and **9** as well as the previously reported $[Cu_5(trz)_3Cl_2]$ exhibit luminescence thermochromism. The spectra are characterized by broad emissions, long lifetimes, and significant Stokes' shifts, characteristic of phosphorescence.

Introduction

Among new classes of materials enjoying widespread contemporary interest, hybrid organic−inorganic materials occupy a prominent position by virtue of their applications to catalysis,[1] optical materials,[2] membranes,[3] and sorption.[4] The diversity of properties associated with these materials reflects a vast compositional range, which allows variations in covalency, geometry, and oxidation states, and a versatile crystalline architecture, which may provide different pore structures, coordination sites, or juxtapositions of functional groups.[5]

Such complex structures, based on a molecular-scale composite of inorganic and organic components, provide the potential for the design of novel functional materials. The inorganic component may provide electrical mobility, un-

* To whom correspondence should be addressed. E-mail: jazubiet@syr.edu. Fax: 315-443-4070 (J.Z.); E-mail: dunbar@mail.chem.tamu.edu. Fax: 979-845-7177 (K.R.D.).

[†] Syracuse University.

[‡] Texas A&M University.

(1) For example, see: (a) Ngo, H. L.; Hu, A. G.; Lin, W. B. *J. Mol. Catal. A* **2004**, *215*, 177. (b) Evans, O. R.; Ngo, H. L.; Lin, W. B. *J. Am. Chem. Soc.* **2001**, *123*, 10395. (c) Vioux, A.; Le Bideau, J.; Mutin, P. H.; Leclercq, D. *Top. Chem. Chem.* **2004**, *232*, 145.

(2) (a) Sanchez, C.; Lebeau, B.; Chaput, F.; Boilot, J. P. *Adv. Mater.* **2003**, *15*, 1969. (b) Evans, O. R.; Lin, W. B. *Chem. Mater.* **2001**, *13*, 3009.

(3) (a) Jannasch, P. *Curr. Opin. Colloid Interface Sci.* **2003**, *8*, 96. (b) Javaid, A.; Hughey, M. P.; Varutbangkul, V.; Ford, D. M. *J. Membr. Sci.* **2001**, *187*, 141. (c) Honma, I.; Nomura, S.; Nakajima, H. *J. Membr. Sci.* **2001**, *185*, 83.

(4) For example, see: (a) Sudik, A. C.; Millward, A. R.; Ockwig, N. W.; Cote, A. P.; Kim, J.; Yaghi, O. M. *J. Am. Chem. Soc.* **2005**, *127*, 7110. (b) Rowsell, J. L. C.; Millward, A. R.; Park, K. S.; Yaghi, O. M. *J. Am. Chem. Soc.* **2004**, *126*, 5666. (c) Kitaura, R.; Kitagawa, S.; Kubtoa, Y.; Kobayashi, T. C.; Kindo, K.; Mita, Y.; Matsuo, A.; Kobayashi, M.; Chang, H.-C.; Ozawa, T. C.; Suzuki, M.; Sakata, M.; Takata, M. *Science* **2002**, *298*, 2358.

10.1021/ic061102e CCC: $33.50
Published on Web 10/18/2006

usual magnetic, dielectric, or optical properties, mechanical hardness, and thermal stability. Similarly, organic molecules offer processability, structural diversity, a range of polarizabilities, and useful luminescence properties.[6,7] Consequently, the combination of the unique features of organic and inorganic compounds in a complementary fashion in hybrid materials may lead to unusual solid-state structures and materials with composite or novel properties, providing access to a vast area of complex, multifunctional materials.

In organic−inorganic hybrid materials, both the inorganic and organic components are integral parts of an extended structure. Two categories of such materials have been identified: metal−organic frameworks (MOFs) or coordination polymers, in which metal atoms or clusters are bridged by polyfunctional organic molecules, and metal oxide hybrids in which metal−oxygen−metal (M−O−M or M−O−M′) arrays are embedded within the architectures.[8,9]

The design of organic−inorganic hybrid materials conceives of the metal, metal cluster, or metal oxide substructure as a node from which rigid or flexible multitopic organic ligands radiate to act as tethers to adjacent nodes in the bottom-up construction of complex extended architectures. While a variety of organic molecules have been investigated as potential tethers, materials incorporating multitopic carboxylates and pyridine ligands have witnessed the most significant development.[5] However, ligands offering alternative tether lengths, different charge-balance requirements, and orientations of donor groups may afford advantages in the design of materials. One such ligand is 1,2,4-triazole and its derivatives, which exhibit an extensively documented ability to bridge metal ions to afford polynuclear compounds.[10−17] The triazoles are members of the polyazaheteroaromatic class of compounds such as pyrazole, imidazole, and tetrazole, which are significant for their technological applications and for their widespread use as bridging ligands. Coordination compounds of 1,2,4-triazoles exhibit unusual structural diversity as a result of the di- and trinucleating properties of the neutral and anionic ligand forms, respectively. Triazoles are readily derivatized, and a number of functionalized compounds are readily accessible.[17−20] Furthermore, the superexchange capacity of the ligand is reflected in the unusual magnetic properties of the complexes.[21−23]

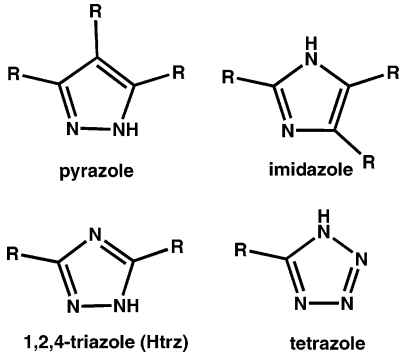

We have recently described the exploitation of hydrothermal synthesis in the preparation of metal/triazolates (trz) with complex framework structures and unusual magnetic properties.[24−26] For materials of the Cu/trz/X system, where X is an anionic component such as OH^-, VO_3^-, or $Mo_4O_{13}^{2-}$, the identity of the anion dramatically influences the structure and properties of the composite materials. In an attempt to explore further the structural consequences of diverse anions on materials of the Cu/trz/X system, we have prepared eight novel phases with X = F^-, Cl^-, Br^-, I^-, or SO_4^{2-}. The structures of $[Cu_3(trz)_4(H_2O)_3]F_2$ (**1**), $[Cu^{II}Cu^{I}(trz)Cl_2]$ (**2**), $[Cu_6(trz)_4Br_2]$ (**3**), $[Cu_6(trz)_4Br]Cu_4Br_4(OH)$ (**4**), $[Cu^{II}Cu^{I}(trz)Br_2]$ (**5**), $[Cu_3(trz)I_2]$ (**6**), $[Cu^{II}Cu^{I}(trz)_2][Cu_3^{I}I_4]$ (**7**), $[Cu_6^{II}Cu_2^{I}(trz)_6(SO_4)_3(OH)_2(H_2O)]$ (**8**), and $[Cu_4(trz)_3]OH\cdot 7.5H_2O$ (**9**·$7.5H_2O$), as well as the magnetic properties of the Cu^{II} species **1** and of the mixed-valence materials **5**, **7**, **8**, and the previously reported $[Cu_3(trz)_3OH][Cu_2Br_4]$, are described. The luminescence properties of the Cu^{I} complexes **3**, **4**, **6**, **9**, and $[Cu_3(trz)_2][Cu_2(trz)(Cl)Cl\cdot 3H_2O$ are also discussed.

(5) The literature on organic−inorganic hybrid materials is voluminous. Some recent reviews and representative articles include the following: (a) Ferey, G.; Mellot-Draznieks, C.; Serre, C.; Millange, F. *Acc. Chem. Res.* **2005**, *38*, 217. (b) Kitagawa, S.; Noro, S. *Compr. Coord. Chem. II* **2004**, *7*, 231. (c) Rao, C. N. R.; Natarajan, S.; Vaidhyanathan, R. *Angew. Chem., Int. Ed.* **2004**, *43*, 1466. (d) Kitagawa, S.; Kitaura, R.; Noro, S.-I. *Angew. Chem., Int. Ed.* **2004**, *43*, 2334. (e) Yaghi, O. M.; O'Keeffe, M.; Ockwig, N. W.; Chae, H. K.; Eddaoudi, M.; Kim, J. *Nature (London)* **2003**, *423*, 705. (f) Lu, J. Y. *Coord. Chem. Rev.* **2003**, *246*, 327. (g) James, S. L. *Chem. Soc. Rev.* **2003**, *32*, 276. (h) Batten, S. R.; Robson, R. *Angew. Chem., Int. Ed.* **1998**, *37*, 1461. (i) Ferey, G. *J. Solid State Chem.* **2000**, *152*, 37. (j) Moulton, B.; Zaworotko, M. J. *Chem. Rev.* **2001**, *101*, 1629. (k) Papaefstathiou, G. S.; MacGillivray, L. R. *Coord. Chem. Rev.* **2003**, *246*, 169. (l) Eddaoudi, M.; Moler, D. B.; Li, H.; Chen, B.; Reineke, T. M.; O'Keeffe, M.; Yaghi, O. M. *Acc. Chem. Res.* **2001**, *34*, 319. (m) O'Keeffe, M.; Eddaoudi, M.; Li, H. Reineke, T.; Yaghi, O. M. *J. Solid State Chem.* **2000**, *152*, 3. (n) Kitaura, R.; Onoyama, G.; Sakamoto, H.; Matsuda, R.; Noro, S.-I.; Kitagawa, S. *Angew. Chem., Int. Ed.* **2004**, *43*, 2684. (o) Hoskins, B. F.; Robson, R. *J. Am. Chem. Soc.* **1990**, *112*, 1546.
(6) Janiak, C. *Dalton Trans.* **2003**, 2781 and references cited therein.
(7) Mitzi, D. B. *Dalton Trans.* **2001**, 1.
(8) Forster, P. M.; Cheetham, A. K. *Top. Catal.* **2003**, *24*, 79.
(9) Hagrman, P. J.; Hagrman, D.; Zubieta, J. *Angew. Chem., Int. Ed.* **1999**, *38*, 2638.
(10) Potts, K. T. *Chem. Rev.* **1961**, *61*, 87.
(11) Klingale, M. H.; Brooker, S. *Coord. Chem. Rev.* **2003**, *241*, 119.
(12) Beckman, U.; Brooker, S. *Coord. Chem. Rev.* **2003**, *245*, 17.
(13) Haasnoot, J. G. *Coord. Chem. Rev.* **2000**, *200−202*, 131.
(14) Chivers, T.; Fu, Z.; Thompson, L. K. *Chem. Commun.* **2005**, 2339.
(15) Zhang, J.-P.; Lin, Y.-Y.; Huang, X.-C.; Chen, X.-M. *J. Am. Chem. Soc.* **2005**, *127*, 5495.
(16) Zhang, J.-P.; Zhang, S.-L.; Huang, X.-C.; Chen, X.-M. *Angew. Chem., Int. Ed.* **2004**, *43*, 206.
(17) Ferrer, S.; Lloret, F.; Bertomeu, I.; Alzuet, G.; Borras, J.; Garcia-Granda, S.; Liu-Gonzalez, M.; Haasnoot, J. G. *Inorg. Chem.* **2002**, *41*, 5821.
(18) Zhou, J.-H.; Cheng, R.-M.; Song, Y.; Li, Y.-Z.; Yu, Z.; Chen, X.-T.; Xue, Z.-L.; You, X.-Z. *Inorg. Chem.* **2005**, *44*, 8011.
(19) Du, M.; Jiang, X.-J.; Zhao, X.-J. *Chem. Commun.* **2005**, 5521.
(20) Zhang, J.-P.; Lin, Y.-Y.; Zhang, W.-X.; Chen, X.-M. *J. Am. Chem. Soc.* **2005**, *127*, 14162.
(21) Kahn, O.; Martinez, C. J. *Science* **1998**, *279*, 44 and references cited therein.
(22) Klingele, M. H.; Boyd, P. D. W.; Moubaraki, B.; Murray, K. S.; Brooker, S. *Eur. J. Inorg. Chem.* **2005**, 910.
(23) Ferrer, S.; van Korringsbruggen, P. J.; Haasnoot, J. G.; Reedijk, J.; Kooijman, H.; Spek, A. L.; Lezama, L.; Arif, A. M.; Miller, J. S. *J. Chem. Soc., Dalton Trans.* **1999**, 4269.
(24) Ouellette, W.; Galan-Mascaros, J. R.; Dunbar, K. R.; Zubieta, J. *Inorg. Chem.* **2006**, *45*, 1909.
(25) Hagrman, P. J.; Bridges, C.; Greedan, J. E.; Zubieta, J. *J. Chem. Soc., Dalton Trans.* **1999**, 2901.
(26) Hagrman, D.; Zubieta, J. *Chem. Commun.* **1998**, 2005.

Experimental Section

General Considerations. All chemicals were used as obtained without further purification: copper(II) sulfate pentahydrate, copper(II) fluoride trihydrate, copper(II) chloride dihydrate, copper(I) bromide, copper(II) bromide, copper(I) iodide, 1,2,4-triazole, and tetrabutylammonium hydroxide were purchased from Aldrich. All syntheses were carried out in 23-mL poly(tetrafluoroethylene)-lined stainless steel containers under autogenous pressure. The reactants were stirred briefly, and initial pH was measured before heating. Water was distilled above 3.0 MΩ in-house using a Barnstead model 525 Biopure Distilled Water Center. The reactions' initial and final pH values were measured using Hydrion pH sticks.

Synthesis of $[Cu_3(trz)_4(H_2O)_3]F_2$ (1). A mixture of $CuF_2 \cdot 3H_2O$ (0.262 g, 1.684 mmol), 1,2,4-triazole (0.0.228 g, 3.330 mmol), and H_2O (10.00 g, 556 mmol) in the mole ratio 0.51:1.00:167 was stirred briefly before heating to 200 °C for 48 h (initial and final pH values of 3.5 and 2.5, respectively). Purple crystals of **1**, suitable for X-ray diffraction, were isolated in 50% yield. IR (KBr pellet, cm^{-1}): 3424(b), 3092(w), 2926(w), 1524(s), 1300(m), 1233(w), 1181(m), 1103(s), 1000(w), 917(w), 876(w), 669(m).

Synthesis of $[Cu_2(trz)Cl_2]$ (2). A solution of $CuCl_2 \cdot 2H_2O$ (0.284 g, 1.666 mmol), 1,2,4-triazole (0.230 g, 3.330 mmol), and H_2O (10.00 g, 556 mmol) in the mole ratio 0.50:1.00:167 was stirred briefly before heating to 180 °C for 48 h (initial and final pH values of 2.0 and 1.5, respectively). Black rods of **2** were isolated in 10% yield. IR (KBr pellet, cm^{-1}): 3134(w), 1633(w), 1513(m), 1290(m), 1171(w), 1103(s), 1051(w), 994(w), 870(m), 652(m).

Synthesis of $[Cu_6(trz)_4Br_2]$ (3). A solution of CuBr (0.243 g, 1.694 mmol), 1,2,4-triazole (0.239 g, 3.460 mmol), and H_2O (10.00 g, 556 mmol) in the mole ratio 0.49:1.00:161 was stirred briefly before heating to 200 °C for 96 h (initial and final pH values of 4.0 and 3.0, respectively). Colorless crystals of **3**, suitable for X-ray diffraction, were isolated in 85% yield. IR (KBr pellet, cm^{-1}): 3102(w), 1503(m), 1275(s), 1155(s), 1077(m), 989(m), 875(m), 652(m).

Synthesis of $[Cu_6(trz)_4Br]Cu_4Br_4(OH)$ (4). A mixture of $CuBr_2$ (0.370 g, 1.657 mmol), 1,2,4-triazole (0.235 g, 3.402 mmol), and H_2O (10.00 g, 556 mmol) in the mole ratio 0.97:1.00:587:9.18 was stirred briefly before heating to 200 °C for 48 h (initial and final pH values of 2.5 and 3.0, respectively). Colorless rods of **4** were isolated in 85% yield. IR (KBr pellet, cm^{-1}): 3455(b), 3102(w), 1508(s), 1280(s), 1207(w), 1160(s), 1084(m), 1000(m), 870(m), 657(s). Anal. Calcd for $C_8H_9N_{12}OCu_{10}Br_5$ (found): C, 7.26 (7.22); H, 0.69 (0.58); N, 12.7 (12.4); Cu, 48.0 (47.8); Br, 30.2 (29.8).

Synthesis of $[Cu_2(trz)Br_2]$ (5). After brief stirring, a mixture of CuBr (0.801 g, 5.580 mmol), 1,2,4-triazole (0.205 g, 2.971 mmol), and H_2O (10.00 g, 556 mmol) in the mole ratio 1.88:1.00:187 was heated to 170 °C for 96 h (initial and final pH values of 3.5 and 2.0, respectively). Black rods of **5** were isolated in 75% yield. IR (KBr pellet, cm^{-1}): 3134(w), 1633(w), 1513(m), 1290(m), 1171(w), 1103(s), 1051(w), 989(w), 875(m), 657(m).

Synthesis of $[Cu_3(trz)I_2]$ (6). A mixture of CuI (0.323 g, 1.696 mmol), 1,2,4-triazole (0.230 g, 3.333 mmol), and H_2O (10.00 g, 556 mmol) in the mole ratio 0.51:1.00:167 was stirred briefly before heating to 200 °C for 48 h (initial and final pH values of 4.0 and 3.5, respectively). Colorless plates of **6** were isolated in 25% yield. IR (KBr pellet, cm^{-1}): 3123(w), 1736(w), 1508(s), 1275(s), 1155(s), 1072(m), 1000(m), 865(m), 652(s).

Synthesis of $[Cu_2(trz)_2][Cu_3I_4]$ (7). After stirring for 10 min, a mixture of CuI (0.322 g, 1.691 mmol), 1,2,4-triazole (0.233 g, 3.373 mmol), and H_2O (10.00 g, 556 mmol) in the mole ratio 0.50:1.00:165 was heated to 180 °C for 72 h. Initial and final pH values of 4.0 and 3.0, respectively, were recorded. Purple crystals of **7,** suitable for X-ray diffraction, were isolated in 35% yield. IR (KBr pellet, cm^{-1}): 3123(w), 1508(s), 1290(m), 1181(m), 1093(s), 1005(w), 870(s), 657(s).

Synthesis of $[Cu_8(trz)_6(SO_4)_3(OH)_2(H_2O)]$ (8). A solution of $CuSO_4 \cdot 5H_2O$ (0.166 g, 0.639 mmol), 1,2,4-triazole (0.047 g, 0.680 mmol), and H_2O (10.00 g, 556 mmol) in the mole ratio 0.94:1.00:818 was stirred briefly before heating to 200 °C for 72 h (initial and final pH values were 2.5 and 2.0, respectively). Green crystals of **8**, suitable for X-ray diffraction, were isolated in 90% yield. IR (KBr pellet, cm^{-1}): 3393(b), 3123(w), 1518(s), 1290(m), 1171(s), 1124(m), 1093(m), 1041(s), 942(m), 891(m), 662(m), 595(m), 475(w).

Synthesis of $[Cu_4(trz)_3]OH \cdot 7.5H_2O$ ($9 \cdot 7.5H_2O$). A solution of $CuSO_4 \cdot 5H_2O$ (0.250 g, 0.963 mmol), 1,2,4-triazole (0.050 g, 0.724 mmol), H_2O (10.00 g, 556 mmol), and tetrabutylammonium hydroxide (40%; 0.050 mL, 0.077 mmol) in the mole ratio 1.33:1.00:768:0.11 was heated at 200 °C for 48 h (initial and final pH values of 2.5 and 3.0, respectively). Colorless rods of **$9 \cdot 7.5H_2O$** were isolated in 85% yield. IR (KBr pellet, cm^{-1}): 3479(b), 3142(w), 1629(m), 1515(s), 1298(m), 1170(s), 1104(s), 1000(w), 881(m), 663(m), 617(m).

X-ray Crystallography. Structural measurements were performed on a Bruker-AXS SMART-CCD diffractometer at low temperature (90 K) using graphite-monochromated Mo Kα radiation ($\lambda_{Mo\ K\alpha} = 0.710\ 73$ Å).[27] The data were corrected for Lorentz and polarization[28] effects and absorption using *SADABS*.[29] The structures were solved by direct methods. All non-H atoms were refined anistropically. After all of the non-H atoms were located, the model was refined against F^2, initially using isotropic and later anistropic thermal displacement parameters. H atoms were introduced in calculated positions and refined isotropically. Neutral atom scattering coefficients and anomalous dispersion corrections were taken from the *International Tables*, Vol. C. All calculations were performed using *SHELXTL* crystallographic software packages.[30]

Compounds **8** and **9** were determined to be nonmerohedral twins from the initial diffraction patterns. The program *Cell_Now*[31] was used to determine that **8** and **9** were composed of two crystal domains, with the second domain rotated by 180° with respect to the first crystal domain. A twin law was created and imported into the *SAINT-PLUS* software package,[32] where the data were corrected for Lorentz and polarization effects and absorption using *TWINABS*.[33] The structures were then solved by direct methods.

Compound **4** exhibited a well-behaved $\{Cu_6(trz)Br\}_n^{n+}$ framework. However, the anionic guests of the framework cavities were highly disordered. The crystallographic model was consistent with a $\{Cu_4Br_3(OH)\}_n$ spiral chain, with isolated Br^- anions disordered along the *z* axis about the special position 0.250, 0.000, and 0.375 at the center of the cavities. The electron density associated with the disordered chain and this anion occupancy is consistent with

(27) *SMART, Data Collection Software*, version 5.630; Bruker AXS Inc.: Madison, WI, 1997−2002.
(28) *SAINT Plus, Date Reduction Software*, version, 6.45A; Bruker AXS Inc.: Madison, WI, 1997−2002.
(29) Sheldrick, G. M. *SADABS*; University of Göttingen: Göttingen, Germany, 1996.
(30) *SHELXTL PC*, version 6.12; Bruker AXS Inc.: Madison, WI, 2002.
(31) Sheldrick, G. M. Cell_Now 1-22-2004; Bruker AXS Inc.: Göttingen, Germany, 2004.
(32) Sheldrick, G. M. *SAINT Plus*, version 6.45; Bruker AXS Inc.: Madison, WI, 1996.
(33) Sheldrick, G. M. *TWINABS: Program for the Empirical Absorption Corrections for Twins*; Bruker AXS Inc.: Madison, WI, 2003.

Table 1. Summary of Crystallographic Data for the Structures of **1**−**8** and **9**·7.5H_2O

	1	**2**	**3**	**4**
empirical formula	$C_4H_7Cu_{1.5}FNO_{1.5}$	$CHClCuN_{1.5}$	$C_8H_8Br_2Cu_6N_{12}$	$C_2H_{2.25}Br_{1.25}Cu_{2.5}N_3O_{0.25}$
fw	277.47	133.02	813.32	331.06
cryst syst	orthorhombic	orthorhombic	triclinic	tetragonal
space group	$Pmn2_1$	$Pnna$	$P\bar{1}$	I_1/acd
a, Å	8.9307(6)	6.7716(4)	7.3624(8)	28.678(1)
b, Å	12.8226(9)	6.8885(5)	8.6798(9)	28.678(1)
c, Å	7.9821(6)	12.3605(8)	14.3089(15)	6.5270(6)
α, deg	90	90	86.401(2)	90
β, deg	90	90	83.160(2)	90
γ, deg	90	90	81.975(2)	90
V, Å	914.1(1)	576.57(7)	898.0(2)	5368.1(6)
Z	4	8	2	32
D_{calcd}, g cm^{-3}	2.016	3.065	3.008	3.277
μ, mm^{-1}	3.518	8.186	11.450	15.226
T, K	90(2)	90(2)	90(2)	90(2)
λ, Å	0.710 73	0.710 73	0.710 73	0.710 73
R1[a]	0.0303	0.0250	0.0436	0.0601
wR2[a]	0.0777	0.0524	0.0696	0.1204
Flack	0.0(4)			

	5	**6**	**7**	**8**	**9**·7.5H_2O
empirical formula	$CHBrCuN_{1.5}$	$C_2H_2Cu_3I_2N_3$	$C_2H_2Cu_{2.5}I_2N_3$	$C_{12}H_{14}Cu_8N_{18}O_{15}S_3$	$C_6H_{22}Cu_4N_9O_{8.5}$
fw	177.48	512.49	480.72	1254.91	610.49
cryst syst	monoclinic	monoclinic	orthorhombic	monoclinic	orthorhombic
space group	$C2/c$	$P2/n$	$Ina2$	$P2_1/c$	$Fdd2$
a, Å	9.500(1)	9.7141(9)	7.4022(4)	7.234(1)	6.5561(6)
b, Å	12.632(2)	4.0899(4)	11.0853(6)	17.393(2)	21.983(2)
c, Å	6.968(1)	21.067(2)	19.293(1)	22.354(2)	39.775(4)
α, deg	90	90	90	90	90
β, deg	131.617(2)	98.896(2)	90	91.61(3)	90
γ, deg	90	90	90	90	90
V, Å	625.1(2)	826.9(1)	1583.1(2)	2937(1)	5732.4(9)
Z	8	4	8	4	16
D_{calcd}, g cm^{-3}	3.772	4.112	4.034	2.838	2.830
μ, mm^{-1}	19.480	15.036	14.398	5.995	5.933
T, K	90(2)	90(2)	90(2)	90(2)	90(2)
λ, Å	0.710 73	0.710 73	0.710 73	0.710 73	0.710 73
R1[a]	0.0202	0.0352	0.0546	0.0840	0.0830
wR2[a]	0.0492	0.0739	0.1348	0.1684	0.1650
Flack					0.0(2)

[a] $R1 = \sum||F_o| - |F_c||/\sum|F_o|$. $wR2 = \{\sum[w(F_o^2 - F_c^2)^2]/\sum[w(F_o^2)^2]\}^{1/2}$.

that calculated by *PLATON*[34] and consistent with duplicate elemental analyses, the average of which are provided above.

Crystallographic details have been summarized in Table 1. Atomic positional parameters, full tables of bond lengths and angles, and anisotropic temperature factors are available in the Supporting Information. Selected bond lengths and angles are given in Table 2.

Results and Discussion

Syntheses. Investigations into the design and discovery of new organic−inorganic hybrid materials[35] are driven by their range of physical properties and their widespread applications to fields as diverse as sorption, catalysis, and molecular electronics. In this respect, it is noteworthy that the existence of naturally occurring, structurally complex minerals has established that hydrothermal synthesis provides a low-temperature pathway for the isolation of open-framework, often metastable, structures from simple inorganic starting materials.[36,37] Most significantly, hydrothermal techniques may be combined with the introduction of organic components,[37] acting as charge-compensating groups, space-filling units, structure-directing agents, and tethers between functional groups or conventional ligands, in the preparation of novel organic−inorganic composites whose structural and physical properties may be substantially modified. The triazolate ligand and its derivatives not only provide effective linkers between metal sites but also are chemically robust and stable under hydrothermal reaction conditions. Triazoles and other polyazaheteroaromatic molecules thus provide attractive alternatives to di- and polytopic carboxylates in the design of organic−inorganic framework materials.[38]

The compounds of this study were prepared in modest to good yields by exploiting the hydrothermal reactions of 1,2,4-triazole with the appropriate copper(I) or copper(II) salt at temperatures in the 180−200 °C range for 48−96 h. The conditions reported in the Experimental Section have been optimized for yields of crystalline product.

In common with previously investigated metal−organic hybrid systems, the hydrothermal chemistry of the materials of the Cu/trz/anion family is remarkably sensitive to variations in reaction conditions. For example, the reaction of $CuCl_2$·2H_2O and triazole in water at 180 °C yields **2**, while the same reactants in the same stoichiometry provided [Cu_3-

(34) Spek, A. L. *PLATON, A Multipurpose Crystallographic Tool*; Utrecht University: Utrecht, The Netherlands, 2005. Spek, A. L. *J. Appl. Crystallogr.* **2003**, *36*, 7.

(35) In addition to their sorptive properties, other properties of inorganic−organic hybrids, specifically MOFs, have been extensively elaborated on in recent years. For example, porosity: (a) Bradshaw, D.; Claridge, J. B.; Cussen, E. J.; Prior, T. J.; Rosseinsky, M. J. *Acc. Chem. Res.* **2005**, *38*, 273. (b) Rosseinsky, M. J. *Microporous Mesoporous Mater.* **2004**, *73*, 15. (c) Cingolani, A.; Galli, S.; Masciocchi, N.; Pandolfo, L.; Pettinari, C.; Sironi, A. *J. Am. Chem. Soc.* **2005**, *127*, 6144. (d) Ohmori, O.; Kawano, M.; Fujita, M. *Angew. Chem., Int. Ed.* **2005**, *44*, 1962. (e) Wu, C.-D.; Lin, W. *Angew. Chem., Int. Ed.* **2005**, *44*, 1958. (f) Lee, E. Y.; Jang, S. Y.; Suh, M. P. *J. Am. Chem. Soc.* **2005**, *127*, 6374. (g) Noro, S.-I.; Kitagawa, S.; Kondo, M.; Seki, K. *Angew. Chem., Int. Ed.* **2000**, *39*, 2082. (h) Wang, Z.; Zhang, B.; Kurmoo, M.; Green, M. A.; Fujiwara, H.; Otsuka, T.; Kobayashi, H. *Inorg. Chem.* **2005**, *44*, 1230. (i) Kim, H.; Suh, M. P. *Inorg. Chem.* **2005**, *44*, 810. (j) Ohmori, O.; Kawano, M.; Fujita, M. *J. Am. Chem. Soc.* **2004**, *126*, 16292. (k) Kitagawa, S.; Kitaura, R. *Comments Inorg. Chem.* **2002**, *23*, 101. (l) Kitaura, R.; Kitagawa, S.; Kubota, Y.; Kobayashi, T. C.; Kindo, K.; Mita, Y.; Matsuo, A.; Kobayashi, M.; Chang, H.-C.; Ozawa, T. C.; Suzuki, M.; Sakata, M.; Takata, M. *Science* **2002**, *298*, 2358. (m) Kitagawa, S.; Kitaura, R.; Noro, S.-I. *Angew. Chem., Int. Ed.* **2004**, *43*, 2334. Chiral separations: (n) Bradshaw, D.; Prior, T. J.; Cussen, E. J.; Claridge, J. B.; Rosseinsky, M. J. *J. Am. Chem. Soc.* **2004**, *126*, 6106. (o) Kepert, C. J.; Prior, T. J.; Rosseinsky, M. J. *J. Am. Chem. Soc.* **2000**, *122*, 5158. (p) Abrahams, B. F.; Jackson, P. A.; Robson, R. *Angew. Chem., Int. Ed.* **1998**, *37*, 2656. Molecular sensing: (q) Halder, G. J.; Kepert, C. J.; Moubaraki, B.; Murray, K. S.; Cashion, J. D. *Science* **2002**, *29*, 1762.

(36) (a) Stein, A.; Keller, S. W.; Mallouk, T. E. *Science* **1993**, *259*, 1558. (b) Laudise, R. A. *Chem. Eng. News* **1987**, Sept 28, 30. (c) Gopalakrishnan, J. *Chem. Mater.* **1995**, *7*, 1265. (d) Whittinghan, M. S. *Curr. Opin. Solid State Mater. Sci.* **1996**, *1*, 227. (e) Weller, M.; Dann, S. E. *Curr. Opin. Solid State Mater. Sci.* **1998**, *3*, 137. (f) Gopalakrishnan, J.; Bhuvanrh, N. S. P.; Rangan, K. K. *Curr. Opin. Solid State Mater. Sci.* **1996**, *1*, 285. (g) Rabenau, A. *Angew. Chem., Int. Ed. Engl.* **1985**, *24*, 1026. (h) Lobachev, A. N. *Crystallization processes under hydrothermal conditions*; Consultants Bureau: New York, 1973. (i) Yoshimura, M.; Suchanek, W. L.; Byrappa, K. *Mater. Res. Soc. Bull.* **2000**, 17. (j) Fing, S.; Xu, R. *Acc. Chem. Res.* **2001**, *34*, 239.

(37) Zubieta, J. Solid-state methods, hydrothermal. *Compr. Coord. Chem. II* **2003**, *1*, 697.

(38) Zhang, J.-P.; Chen, X.-M. *Chem. Commun.* **2006**, 1689.

Table 2. Summary of Structural Characteristics of the Compounds of This Study and Related Materials

compound	coordination geometry[a]	Cu−N	Cu−X	polymeric substructure
		I. Cu^{I} Species		
$[Cu_6(trz)_4Br_2]$ (**3**)	linear, $\{N_2\}$ (×2)	1.870(3)−1.884(3) 1.878(4), ave		$\{Cu(trz)\}_n$ network (2-D)
	trigonal planar, $\{N_2I\}$ (×3)	1.894(3)−1.908(3) 1.900(4), ave	2.6254(7)−2.6962(7) 2.6676(8), ave	
	trigonal planar, $\{N_2I\}$ (×1)	1.923(3), 1.941 (3)	2.4515(7)	
$[Cu_6(trz)_4]Br]Cu_4Br_4(OH)$ (**4**)	linear, $\{N_2\}$ (×2)	1.871(5)−1.886(5) 1.878(6), ave		$\{Cu_6(trz)_4\}_n^{2n+}$ framework (3-D)
$[Cu_3(trz)I_2]$ (**6**)	linear (×2)	1.853(5)−1.877(5) 1.865(5), ave		$\{Cu(trz)\}_n$ chains and $\{Cu(I)\}_n$ chains
	tetrahedral, $\{NI_3\}$ (×1)	1.998(5)	2.5962(8), 2.6632(8), 2.7219(8)	
	tetrahedral, $\{I_4\}$ (×1)		2.6832(8), 2.6819(8), 2.6202(8), 2.6312(8)	
$[Cu_4(trz)_3]OH·7.5H_2O$ (**9**)	linear, $\{N_2\}$ (×4)	1.845(9)−1.913(8) 1.87099), ave		$\{Cu_4(trz)_3\}_n^{n+}$ framework (3-D)
	trigonal planar, $\{N_3\}$ (×2)	1.951(8)−2.036(10) 1.977(9), ave		
$[Cu_3(trz)_2][Cu_2(trz)Cl]$-Cl·$3H_2O$	linear, $\{N_2\}$, Cu^{I}	1.874(4)−1.992(9) 1.932(7), ave		$\{Cu_3(trz)_2\}_n^{n+}$ networks (2-D) and $\{Cu_2(trz)Cl\}_n$ chains
	linear $\{NCl\}$, Cu^{I}	1.885(8)	2.660(5)	
		II. Cu^{II} Species		
$[Cu_3(trz)_4(H_2O)_3]F_2$ (**1**)	square pyramidal, $\{N_4O\}$ (×3)	1.981(3)−1.994(3) 1.824(4), ave	2.257(3)−1.412(4) 2.346(4), ave	$\{Cu_3(trz)_4(H_2O)\}_n^{2n+}$ framework (3-D)
$[Cu_3(trz)_3(OH)_3(H_2O)_4]$· $4.5H_2O$	octahedral, $\{N_3O_3\}$, Cu^{II}	1.972(2)−2.004(2) 1.983(2), ave	2.029(1)−2.070(5) 2.056(3), ave	$\{Cu_3(trz)_3(OH)_3(H_2O)_4\}_n$ framework (3-D)
		III. Cu^{I}/Cu^{II} Species		
$[Cu_2(trz)Cl_2]$ (**2**)	octahedral, $\{N_2Cl_4\}$, Cu^{II}	1.937(2) (×2)	2.4095(6) (×2), 2.7403(6) (×2)	$\{Cu_2Cl_2\}_n^{n+}$ networks (2-D)
	trigonal planar, $\{NCl_2\}$, Cu^{I}	1.928(3)	2.2785(6) (×2)	
$[Cu_2(trz)Br_2]$ (**5**)	square pyramidal, $\{N_2Br_3\}$, Cu^{II}	1.945(2) (×2)	2.5381(4) (×1), 2.8814(4) (×2)	$\{Cu(trz)Cl_2\}_n^{n-}$ chains
	trigonal planar, $\{NBr_2\}$, Cu^{I}	1.937(3)	2.4161(5) (×2)	
$[Cu_2(trz)_2][Cu_3I_4]$ (**7**)	square planar, $\{N_4\}$, Cu^{II}	1.971(8) (×2), 2.006(9) (×2)		$\{Cu_2(trz)_2\}_n^{n+}$ framework (3-D) and $\{Cu_3I_4\}_n^{n-}$ chain
	linear, $\{N_2\}$, Cu^{I}	1.833(9), 1.851(10)		
	trigonal planar, $\{I_3\}$, Cu^{I}		2.522(8)−2.838(9) 2.666(11), ave	
$[Cu_8(trz)_6(SO_4)_3(OH)_2$	square planar, $\{N_2O_2\}$ (×2), Cu^{II}	1.934(8)−1.969(8)	1.939(7)−2.001(6)	$\{Cu_4(trz)_3(OH)\}_n^{2n+}$ networks (2-D)
$(H_2O)]$ (**8**)		1.955(8), ave.	1.970(8), ave.	
	square pyramidal, $\{N_3O_2\}$ (×2), Cu^{II}	1.995(7)−2.011(6)	2.018(6), ave (basal)	
		2.001(8), ave	2.163(6), ave (axial)	
	square pyramidal, $\{N_2O_3\}$ (×1), Cu^{II}	1.937(8), 1.958(9)	1.979(7), ave (basal)	
			2.225(7) (axial)	
	octahedral, $\{N_2O_4\}$ (×1), Cu^{II}	1.958(9), 1.965(8)	2.019(8), ave (equatorial) 2.298(8), ave (axial)	
	linear, $\{N_2\}$ (×2), Cu^{I}	1.857(8)−1.869(9) 1.865(9), ave		
$[Cu_3(trz)_3(OH)][Cu_2Br_4]$	square planar, $\{N_3O\}$, Cu^{II}	1.969(8)−1.973(9) 1.970(10), ave	2.043(8)	$\{Cu_3(trz)_3(OH)_n^{2n+}$ framework (3-D) and $\{Cu_2Br_4\}_n^{2n-}$ framework (3-D)
	tetrahedral, $\{Br_4\}$, Cu^{I}		2.361(8)−2.764(10) 2.550(9), ave	

$(trz)_2][Cu_2(trz)Cl]Cl·3H_2O$ at 200 °C.[39] Quite remarkably, the Cu/trz/Br subset is represented by four materials. The hydrothermal reaction of CuBr with triazole at 200 °C for 96 h produced **3**, while adjusting the Cu:Br ratio from 1:2 to ca. 2:1 and lowering the temperature to 180 and 170 °C yielded the phases $[Cu_3(trz)_3OH][Cu_2Br_4]$ and the mixed-valence species **5**, respectively. When the Cu^{II} starting material $CuBr_2$ was used, reduction occurred in the hydrothermal medium to produce the Cu^{I} species **4**. Mixed valence is a common occurrence in the hydrothermal chemistry of this series of compounds and is manifested in materials **2**, **5**, **7**, and **8**. The only exclusively Cu^{II} species of the study is the fluoride **1**.

The Cu/trz/I subset also exhibits high- and low-temperature phases. Thus, the reaction of CuI and triazole at 200 °C produces the Cu^{I} material **6**, while the reaction carried out at 180 °C yields the mixed-valence **7**.

When $CuSO_4·5H_2O$ is used as the Cu source, three phases have been identified; however, sulfate incorporation into the framework is observed only in a single instance. Reaction of copper sulfate with triazole at 200 °C for 72 h yields the mixed-valence **8**; in contrast, when the reaction time is 48 h, the Cu^{II} species $[Cu_3(trz)_3(OH)_3(H_2O)_4]·4.5H_2O$ was isolated. When hydroxide was introduced to adjust the reaction pH, the Cu^{I} phase **9**·$7.5H_2O$ was observed.[39] As

(39) Ouellette, W.; Yu, M. H.; O'Connor, C. J.; Hagrman, D.; Zubieta, J. *Angew. Chem., Int. Ed.* **2006**, *45*, 3497.

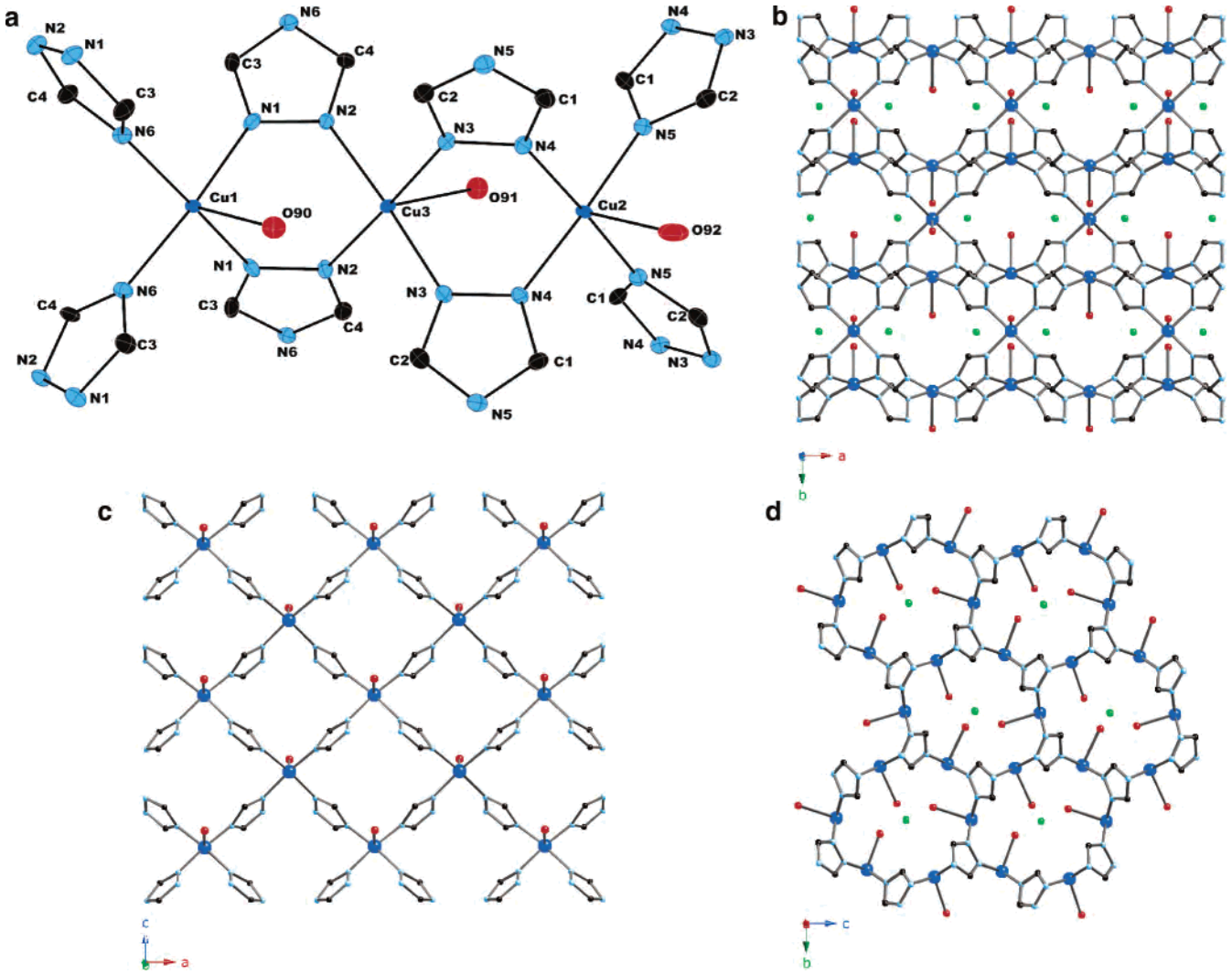

Figure 1. (a) ORTEP view of the structure of **1**, showing the atom-labeling scheme and 50% thermal ellipsoids. (b) View of the structure of **1** in the *ab* plane. Color code: Cu, dark blue; O, red; N, light blue; C, black; F, green. This color scheme is used throughout. (c) View of the structure in the *ac* plane. (d) View of the 20-membered rings that define the cavities occupied by the fluoride anions.

noted previously, under hydrothermal conditions, nitrogenous ligands are effective reducing agents; consequently, mixed-valence and fully reduced metal centers are not uncommon in the hydrothermal products.

The optimal pH range for syntheses of the compounds of this study is 2.0−4.0. A lower reaction pH failed to provide crystalline products, whereas basic pH conditions resulted in ligand decomposition.

In all compounds **1**−**9** of this study and of the Cu/trz/X species previously described,[39,40] the ligand is present in the deprotonated triazolate form and functions as a tripodal linker. Presumably, a shift in pK_a of acidic species under hydrothermal conditions occurs in a manner analogous to that of the shift in pK_a of water,[41] which may preclude the possibility of isolating compounds containing the neutral form Htrz from Cu/Htrz/X systems.

The IR spectra of the complexes exhibit a series of medium-to-strong-intensity bands in the 650−1525 cm^{-1} range, the most prominent of which are four bands in the ranges 1500−1525, 1230−1290, 1160−1180, and 650−675 cm^{-1}, attributed to the triazolate ligand. In addition, compounds **1**, **4**, **8**, and **9** possess a broad, strong feature in the 3400−3500-cm^{-1} range assigned to ν(O−H) of water. The spectra of the remaining phases **2**, **3**, and **5**−**7** show no features at frequencies greater than 3140 cm^{-1}, consistent with the absence of water.

Structural Studies. The complex three-dimensional structure of the fluoride derivative **1** is shown in Figure 1b, projected onto the crystallographic *ab* plane. As illustrated in Figure 1c, each square-pyramidal Cu^{II} site coordinates to four triazolate groups in the basal plane and to an apical aqua ligand. Each triazolate ligand links two Cu^{II} sites in the *ac* plane through the N1 and N4 donor groups and uses the third N donor to link to Cu sites above and below this plane, so as to establish the three-dimensional connectivity. The bonding pattern produces square-grid motifs parallel to the *ac* plane, with the aqua ligands disposed in an alternating fashion above and below the planes. These layered substructures are connected through the second Cu^{II} site and stacked

(40) Chesnut, D. J.; Kusnetzow, A.; Birge, R.; Zubieta, J. *Inorg. Chem.* **1999**, *38*, 5484.
(41) Sweeton, F. H.; Mesmer, R. E.; Baes, C. F., Jr. *J. Solution Chem.* **1974**, *3*, 191.

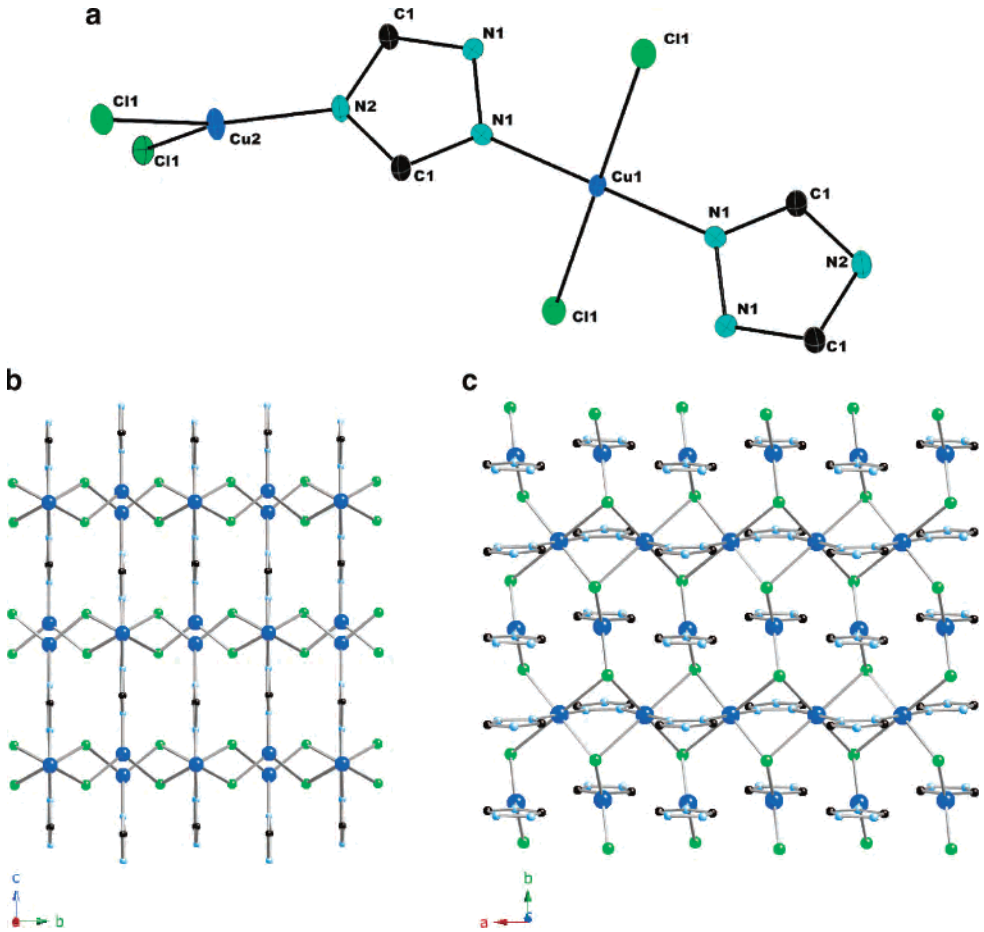

Figure 2. (a) ORTEP view of the structure of **2**, showing the atom-labeling scheme and 50% thermal ellipsoids. (b) View of the structure of **2** in the *bc* plane. (c) Two-dimensional substructure of **2** in the *ab* plane.

perpendicularly to the *b* axis with an interlayer repeat of 7.3 Å. This second Cu^{II} site is distinguished from the layer-embedded site by bonding exclusively to the N2 sites of four triazolate ligands. The connectivity pattern also results in Cu triads, with Cu···Cu vectors parallel to the *b* axis when projected onto the *ab* plane. These trinuclear substructures appear to dominate the magnetic properties of **1** as noted below.

The connectivity pattern produces several embedded cyclic substructures. As shown in Figure 1b, one such motif is a $\{Cu-N-C-N-\}_4$ 16-membered heterocyclic ring, containing two Cu atoms of each type. There is also a second $\{Cu-N-C-N-\}_4$ ring in the *ac* plane that contains only the first type of Cu sites. In addition, where the structure is viewed parallel to the *a* axis as in Figure 1d, a 20-membered $\{Cu-N-C-N-Cu-N-C-N-Cu-N-N-\}_2$ ring is revealed. The fluoride anions occupy the cavities formed by these rings and engage in hydrogen bonding to the aqua ligands.

As shown in Figure 2b, the structure of $[Cu^{II}Cu^{I}(trz)Cl_2]$ (**2**) is also three-dimensional but is constructed from six-coordinate Cu^{II} and three-coordinate CuI sites. The structure may be described as $\{Cu_2Cl_2\}_n^{n+}$ two-dimensional networks parallel to the *ab* plane, linked through triazolate ligands and stacking parallel to the *c* axis. The two-dimensional substructure, shown in Figure 2c, is constructed from $\{Cu^{II}(trz)Cl_2\}_n^{n-}$ chains, bridged by the Cu^{I} sites. Each Cu^{II} site of the chain exhibits distorted octahedral $\{CuCl_4N_2\}$ geometry. The chloride ligands adopt a μ^3-bridging mode, linking two Cu^{II} sites of the chain and a Cu^{I} site. Each Cu^{I} center bridges two adjacent $\{Cu(trz)Cl_2\}_n^{n-}$ chains through chloride ligands and bonds to the N4 donor of a triazolate ligand, which, in turn, bridges to an adjacent network substructure. The Cu^{I} site thus exhibits distorted trigonal-planar $\{Cu^{I}Cl_2N\}$ geometry, with a Cl−Cu−Cl angle of 102.14(5)°. Each triazolate ligand bridges Cu^{II} sites of the chains through the N1 and N2 donors and directs the N4 donor to a Cu^{I} center of an adjacent layer.

The structure of the mixed-valence **2** is distinct from that of the previously described Cu^{I} analogue $[Cu_3(trz)_2][Cu_2(trz)Cl]Cl{\cdot}3H_2O$, which is constructed from network and chain substructures. In this latter case, the network substructure $\{Cu_3(trz)_2\}_n^{n+}$ exhibits exclusively two-coordinate $\{CuN_2\}$ sites. In contrast, the chain contains two distinct two-coordinate sites $\{CuN_2\}$ and $\{CuNCl\}$.

The Cu^{I} material **3** is also three-dimensional, as illustrated in Figure 3b. The structure exhibits a complex connectivity of three-coordinate Cu^{I} sites, defined by bonding to two triazolate N donors and a Br, and of diagonally coordinated Cu^{I} sites with the $\{CuN_2\}$ environment. The three-dimensional structure may be described in terms of two-dimensional subunits linked through one-dimensional substructures. The layer motif, illustrated in the *bc* plane in

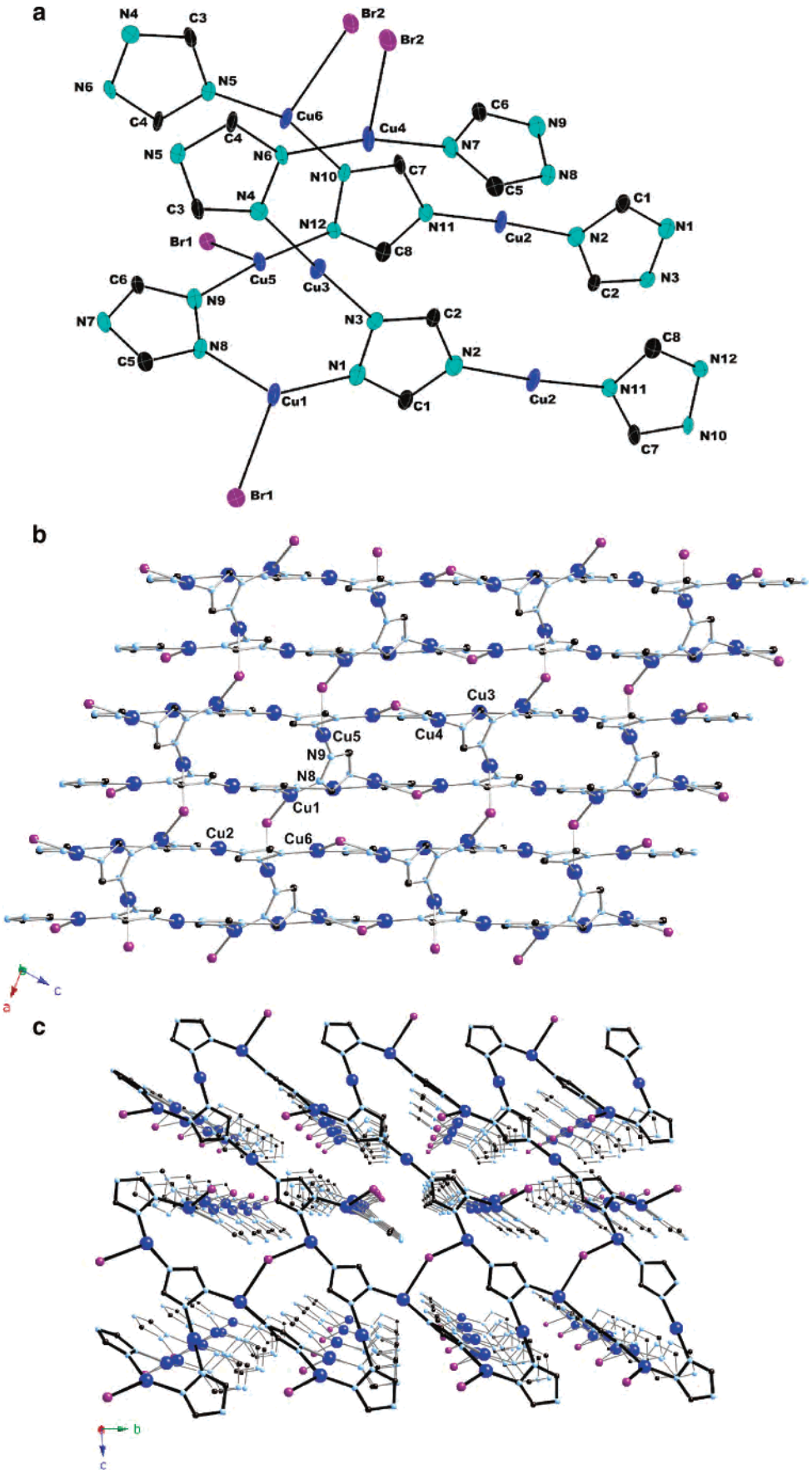

Figure 3. (a) ORTEP view of the structure of **3**, showing the atom-labeling scheme and 50% thermal ellipsoids. (b) Ball-and-stick representation of the structure of **3** in the *ac* plane. (c) Perspective view of the layer substructure of **3**.

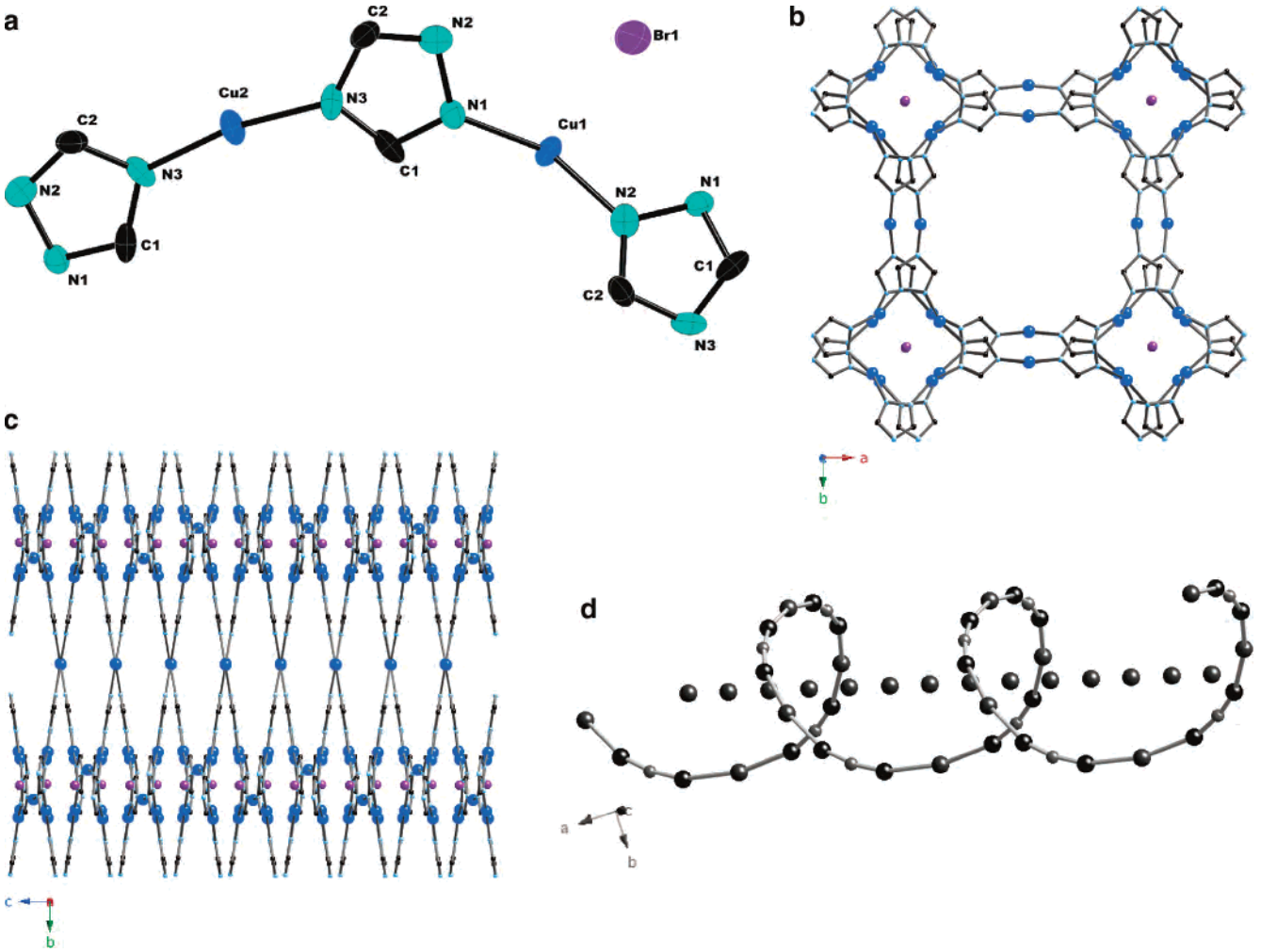

Figure 4. (a) ORTEP view of the structure of **4**, showing the atom-labeling scheme and 50% thermal ellipsoids. (b) View of the structure of **4** in the *ab* plane. (c) Three-dimensional structure of **4** in the *bc* plane. (d) View of the contents of the channels: the $\{Cu_4Br_3(OH)\}_n$ spiral and the Br^- anions at the center of the channel.

Figure 3c, consists of $\{Cu(trz)\}_n$ layers of Cu^I sites bridged through the triazolate N donors, which are cross-linked through an exo-chain bromine. Every fourth triazolate of the chains linked through the N1 and N4 sites engages in bonding to this bridging bromide. In addition to the two-coordinate Cu sites, the chain contains a three-coordinate $\{CuN_2Br\}$ site. The bromine ligand to this site participates in bridging to the exo-chain Cu site, which also exhibits distorted trigonal-planar geometry.

The triazolate group bound to Cu1 uses the N1 and N2 nitrogen sites to bridge to the Cu sites of the chain substructure, shown in Figure 3b. The nitrogen sites N8 and N9 of the chain also link to these one-dimensional substructures.

A second copper bromide phase $[Cu_6(trz)_4]Br]Cu_4Br_4(OH)$ (**4**) consists of an open-framework three-dimensional cationic unit $\{Cu_6(trz)_4Br\}_n^{n+}$ entraining a one-dimensional $\{Cu_4Br_5\}_n^{n-}$ substructure. As shown in Figure 4b, the cationic framework is constructed from $\{Cu_4(trz)_4\}$ rings linked through exocyclic Cu^I sites into a three-dimensional framework. The Cu^I sites of the rings are bridged through the N1 and N2 sites of the four triazolate ligands to produce a $\{Cu_4N_8\}$ heterocycle. The remaining N4 donor at each triazolate is bonded to the two-coordinate exocyclic Cu^I sites, each of which bridges two $\{Cu_4(trz)_4\}$ clusters. Consequently, each ring is bridged by the exocyclic Cu sites to four adjacent rings to produce a square-grid pattern in the *ab* plane. However, when the structure is reviewed parallel to the N−Cu−N axes of the exocyclic Cu sites, it is revealed that adjacent clusters along the *a* axis (and *b* axis) are rotated by 26° with respect to each other to produce the interlocking three-dimensional framework shown in Figure 4c. Careful inspection also manifests the presence of two identical, interpenetrating three-dimensional grid works.

This connectivity pattern generates two cavities. The smaller, which is produced by the stacking of $\{Cu_4(trz)_4\}$ rings, accommodates one crystallographically distinct Br^- anion. These anions stack parallel to the *a* axis and are displaced from the centroids of the $\{Cu_4(trz)_4\}$ planes by 1.38 Å. The second cavity is generated by the linking of four $\{Cu_4(trz)_4\}$ rings by four exocyclic Cu sites to generate a $[\{Cu_4(trz)_4\}Cu]_4^{4+}$ ring of approximate dimensions 13.0 Å × 13.0 Å. This latter cavity is occupied by a highly disordered $\{Cu_4Br_3(OH)\}_n$ spiral chain, shown in Figure 4d, and a Br^- anion at the center of the cavity, disordered along the crystallographic *c* axis.

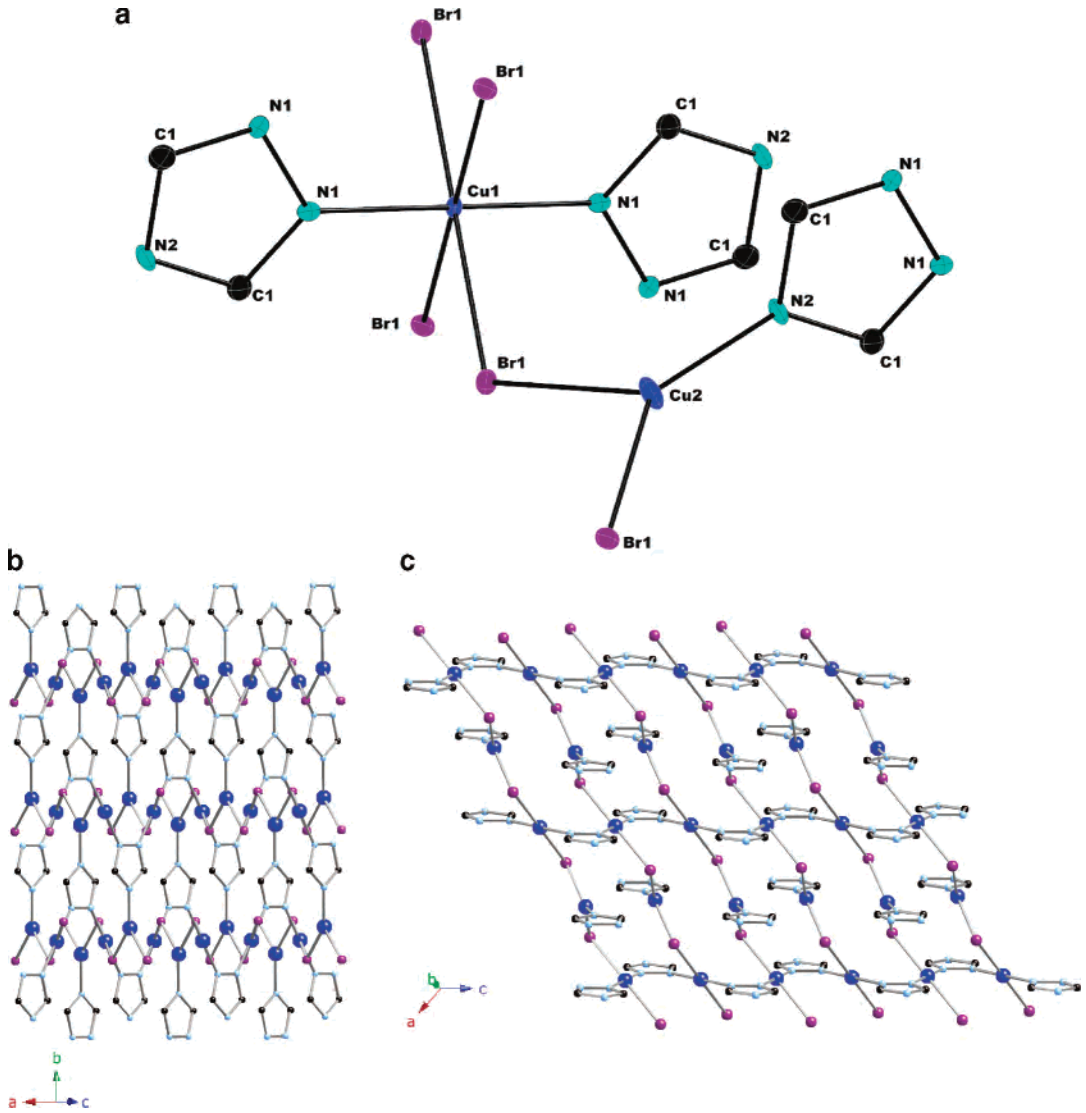

Figure 5. (a) ORTEP view of the structure of **5**, showing the atom-labeling scheme and 50% thermal ellipsoids. (b) View of the three-dimensional structure of **5**. (c) Structure of **5** in the *ac* plane.

A third copper bromide phase $[Cu^{II}Cu^{I}(trz)Br_2]$ (**5**) is a mixed-valence Cu^{I}/Cu^{II} species. As shown in Figure 5b, the three-dimensional structure of **5** exhibits a gross profile in the *ab* plane similar to that described for **2**. However, the structural differences are revealed when the framework of **5** is viewed in the *ac* plane (Figure 5c). In contrast to the six-coordinate Cu^{II} sites of **2**, the Cu^{II} sites of **5** are four-coordinate, $\{CuN_2Br_2\}$. The network substructure of **5** may be described as$\{CuBr\}_n$ chains linked in the plane through N1 and N2 donors of the triazolate ligands at alternating Cu sites. The remaining Cu sites bond to the N4 positions of triazolates from adjacent layers.

The first of the copper iodide materials **6** is a Cu^{I} phase with a three-dimensional structure, shown in Figure 6b. The structure is constructed from $\{CuI\}_n$ chains running parallel to the *b* axis, linked through $\{Cu(trz)\}_n$ chains into a framework structure. The copper iodide substructure, shown in Figure 6c, consists of a double ribbon, each constructed from $\{Cu_3I_3\}$ rings fused at opposite Cu−I edges. These ribbons are, in turn, linked through Cu−I bonds at each Cu site to produce the double-ribbon motif. Alternatively, the copper iodide substructure may be described as $\{Cu_6I_6\}$ drums with six rhombic faces, fused at two opposite faces. There are two distinct distorted tetrahedral Cu^{I} sites. The first exhibits $\{CuI_4\}$ coordination geometry, while the second bonds to three I atoms and to an exocyclic triazolate ligand through an N1 site.

The triazolates projecting from the $\{CuI\}_n$ chain parallel to the *ac* plane use their N2 and N4 donors to bond to the third Cu site. This results in folded $\{Cu(trz)\}_n$ chains whose axes run perpendicular to the axes of the $\{CuI\}_n$ chain substructures. The Cu sites of the $\{Cu(trz)\}_n$ chains exhibit diagonal coordination, with N−Cu−N angles of 180.0° and 164.9(3)°.

The mixed-valence copper iodide phase $[Cu^{II}Cu^{I}(trz)_2]$-$[Cu_3^{I}I_4]$ (**7**) consists of two substructures, a three-dimensional cationic subunit $\{Cu_2(trz)_2\}_n^{n+}$ and a one-dimensional anionic chain $\{Cu_3I_4\}_n^{n-}$ (Figure 7b). The framework substructure is constructed from square-planar Cu^{II} sites and linearly coordinated Cu^{I} sites. The Cu^{II} centers coordinate to the N1/N2 sites of four triazolate ligands, each of which bridges two Cu^{II} sites to form chains running parallel to the *a* axis.

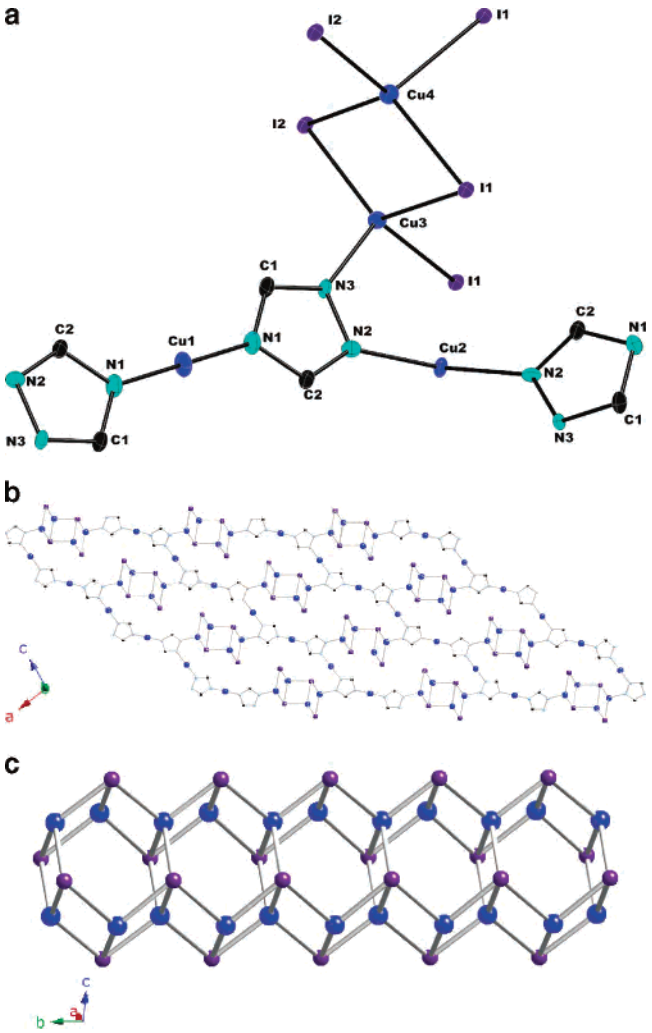

Figure 6. (a) ORTEP view of the structure of **6**, showing the atom-labeling scheme and 50% thermal ellipsoids. (b) Structure of **6** in the *ac* plane, parallel to the axis of the $\{CuI\}_n$ chains. (c) View of the $\{CuI\}_n$ chain of **6**.

However, the $\{Cu(trz)_2\}$ ribbon is not planar, but rather the triazolate planes form angles of 120.0° at a Cu site and 60.0° at adjacent sites, as illustrated in Figure 7c. The N4 positions of each triazolate ligand bond to the Cu^{I}I sites, each of which is two-coordinate and bridges adjacent $\{Cu(trz)_2\}$ chains. The result of this interconnectivity is to generate a three-dimensional framework with a rhombic grid pattern when projected onto the *bc* plane. The most noteworthy characteristic of the grid substructure is the presence of $\{Cu_4^{II}Cu_4^{I}(trz)_8\}^{4+}$ rhombs of approximate dimensions 11.0 Å × 19.3 Å.

The channels formed by the $\{Cu_2(trz)_2\}_n^{n+}$ framework are occupied by the anionic $\{Cu_3I_4\}_n^{n-}$ chains, which run parallel to the *a* axis. As shown in Figure 7d, these chains are constructed from trigonal-planar Cu^{I} sites. The backbone of this one-dimensional substructure is a zigzag $\{CuI\}_n$ chain. Each Cu^{I} site of this motif bonds to two bridging iodide anions and to a terminally coordinated iodide. The iodide atoms of the chain participate in bridging to a third Cu^{I} site, each of which supports two terminal iodine ligands.

The presence of two distinct substructures in **7** is reminiscent of the structure of $[Cu_3(trz)_3OH][Cu_2Br_4]$, which consists of a three-dimensional cationic subunit $\{Cu_3(trz)_3OH\}_n^{2n+}$ and a three-dimensional anionic component $\{CuBr_2\}_n^{n-}$. However, in contrast to **7**, which exhibits a mixed-valence cationic substructure, the Cu sites of the $\{Cu_3(trz)_3OH\}_n^{2n+}$ subunit of $[Cu_3(trz)_3OH][Cu_2Br_4]$ are exclusively Cu^{II}.

The introduction of a dinegative anion constituent provides the complex three-dimensional structure $[Cu_6^{II}Cu_2^{I}(trz)_6(SO_4)_3(OH)_2(H_2O)]$ (**8**), shown in Figure 8. The framework is constructed of layers of $\{Cu_3(trz)_3(\mu^3\text{-}OH)\}^{2+}$ clusters, linked through Cu^{I} sites or triazolate bridges; the layers are bridged, in turn, by the SO_4^{2-} ligands to provide extension in three dimensions.

Within the layer substructure, there are chains of clusters running parallel to the *b* axis that are linked through triazolate groups bonding to Cu sites of the clusters through the N4 positions. These chains are connected to adjacent chains through Cu^{I} sites, bonding to the two remaining triazolate N4 sites of each cluster.

The cluster motifs $\{Cu_3(trz)_3(\mu^3\text{-}OH)\}^{2+}$ exhibit the same geometry as that previously observed in the structures of $[Cu_3(OH)_3(trz)_3(H_2O)_4]\cdot 4.5H_2O$ and of $[Cu_3(trz)_3(\mu^3\text{-}OH)][Cu_2Br_4]$[39] and several trinuclear Cu^{II} molecular compounds.[42,43] Thus, each Cu site of the trinuclear clusters bonds to two N donors of cluster triazolate groups and the μ^3-OH group in forming the capped, triangular motif. However, in the case of $[Cu_3(OH)_3(trz)_3(H_2O)_4]$, all Cu^{II} sites are "4 + 2" axially distorted six-coordinate through additional bonding to an N4 donor site from a triazolate group of an adjacent cluster and either two aqua ligands or an aqua ligand and an OH^- group in the axial positions. One consequence of this bonding pattern is that each $\{Cu_3(trz)_3(\mu^3\text{-}OH)(OH)_2(H_2O)_4\}$ cluster of this latter structure links directly to six adjacent clusters in forming the three-dimensional open framework. In contrast, the clusters of **8** participate in a single direct interaction with a triazolate N4 donor from a neighboring cluster, producing the one-dimensional motif described above. Consequently, each cluster of **8** bridges to four adjacent clusters, two through direct N4−Cu interactions in the chain and two through the Cu^{I} sites. This connectivity results in a two-dimensional Cu/trz/OH^- substructure with mixed-valent Cu^{I}/Cu^{II} sites for **8**, in contrast to the three-dimensional Cu/trz/OH^- structure with exclusively Cu^{II} sites adopted by $[Cu_3(trz)_3(OH)_3(H_2O)_4]\cdot 4.5H_2O$.

Furthermore, there are two distinct trinuclear clusters in **8**, as defined by the exocyclic ligation patterns. The first ring exhibits a square-planar Cu site and two square-pyramidal sites. Because all Cu sites of the clusters bond endocyclically to two triazolate donors and an OH^- group, the four-coordinate site is defined by exocyclic bonding to a sulfate O donor, while one five-coordinate site bonds to two O donors from different sulfate groups and the other square-pyramidal site enjoys coordination to a triazolate N4 donor and to a sulfate O. The second cluster type exhibits a

(42) Casaris, M.; Corvaja, C.; Di Nicola, C.; Falcomer, D.; Franco, L.; Monari, M.; Pandolfo, L.; Pettinari, C.; Piccinelli, F. *Inorg. Chem.* **2005**, *44*, 6265 and references cited therein.
(43) Mezei, G.; McGrady, J. E.; Raptis, R. G. *Inorg. Chem.* **2005**, *44*, 7271 and references cited therein.

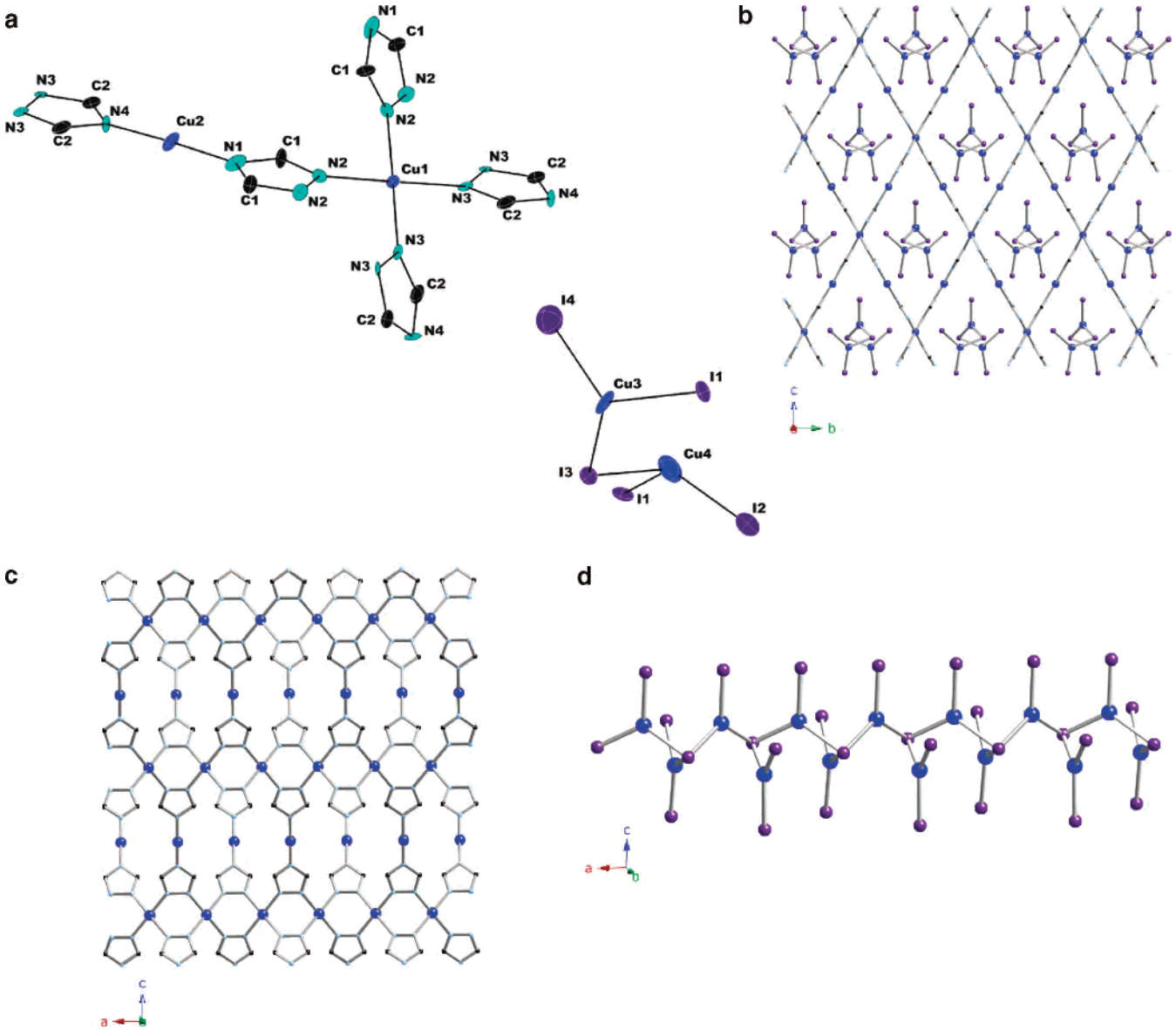

Figure 7. (a) ORTEP view of the structure of **7**, showing the atom-labeling scheme and 50% thermal ellipsoids. (b) View of the structure of **7** in the *bc* plane, parallel to the $\{Cu_3I_4\}_n^{n-}$ chain axis. (c) $\{Cu_2(trz)_2\}_n^{n+}$ substructure of **7** in the *ac* plane. (d) $\{Cu_3I_4\}_n^{n-}$ chain substructure of **7**.

square-planar site, a square-pyramidal site, and a "4 + 2" axially distorted six-coordinate site. The exocyclic bonding is defined by a sulfate O for the four-coordinate site, a sulfate O and a triazolate N4 donor for the second site, and two O donors from different sulfate groups and an aqua ligand for the distorted octahedral site. The five- and six-coordinate sites are bridged by a sulfate group.

The structure of the Cu^I species **9**·$7.5H_2O$, shown in Figure 9, is also three-dimensional. The structure is best described as $\{Cu_3(trz)_3\}$ clusters linked through trigonal-planar exocyclic Cu^I sites to six adjacent triangular clusters. The Cu_3 clusters are grossly similar to those previously reported for $[Cu_3(OH)_3(trz)_3(H_2O)_4]$·$4.5H_2O$ and for $[Cu_8(trz)_6(SO_4)_3(OH)_2(H_2O)$. However, the Cu sites of the triangular clusters of the latter materials are Cu^{II} centers exhibiting square-planar, square-pyramidal, or octahedral geometries, while those of **9** are Cu^I with linear $\{CuN_2\}$ geometries, defined by the N1 and N2 sites of the bridging triazolate ligands. The μ^3-OH group of the Cu^{II} species is not present in the Cu^I material. Each triazolate N4 donor of a cluster bonds to an exocyclic Cu^I site. Each of these trigonal-planar Cu centers links a given cluster to two adjacent clusters.

The connectivity patterns of $\{Cu_3(trz)_3(OH)\}^{2+}$ clusters of $[Cu_3(OH)_3(trz)_3(H_2O)_4]$·$4.5H_2O$ and **8** and of the $\{Cu_3(trz)_3\}$ cluster of **9** are compared in Figure 10. In the case of the Cu^{II} species $[Cu_3(OH)_3(trz)_3(H_2O)_4]$·$4.5H_2O$, each triangular cluster is directly linked through Cu−N4−triazolate bridges to six adjacent clusters. In contrast, each cluster of compound **8** is linked to two adjacent clusters through Cu−N4−triazolate bonds and to two additional clusters through two-coordinate Cu^I sites. Thus, in $[Cu_3(OH)_3(trz)_3(H_2O)_4]$·$4.5H_2O$, all three Cu cluster sites bond to N4−triazolate nitrogen donors of adjacent clusters, while for **8**, only one Cu site of each cluster engages in this direct connectivity. For compound **9**·$7.5H_2O$, the Cu^I sites of the triangular clusters do not engage in exocyclic bonding at all, such that the connectivity is established exclusively through the exocyclic $\{CuN_3\}$ sites.

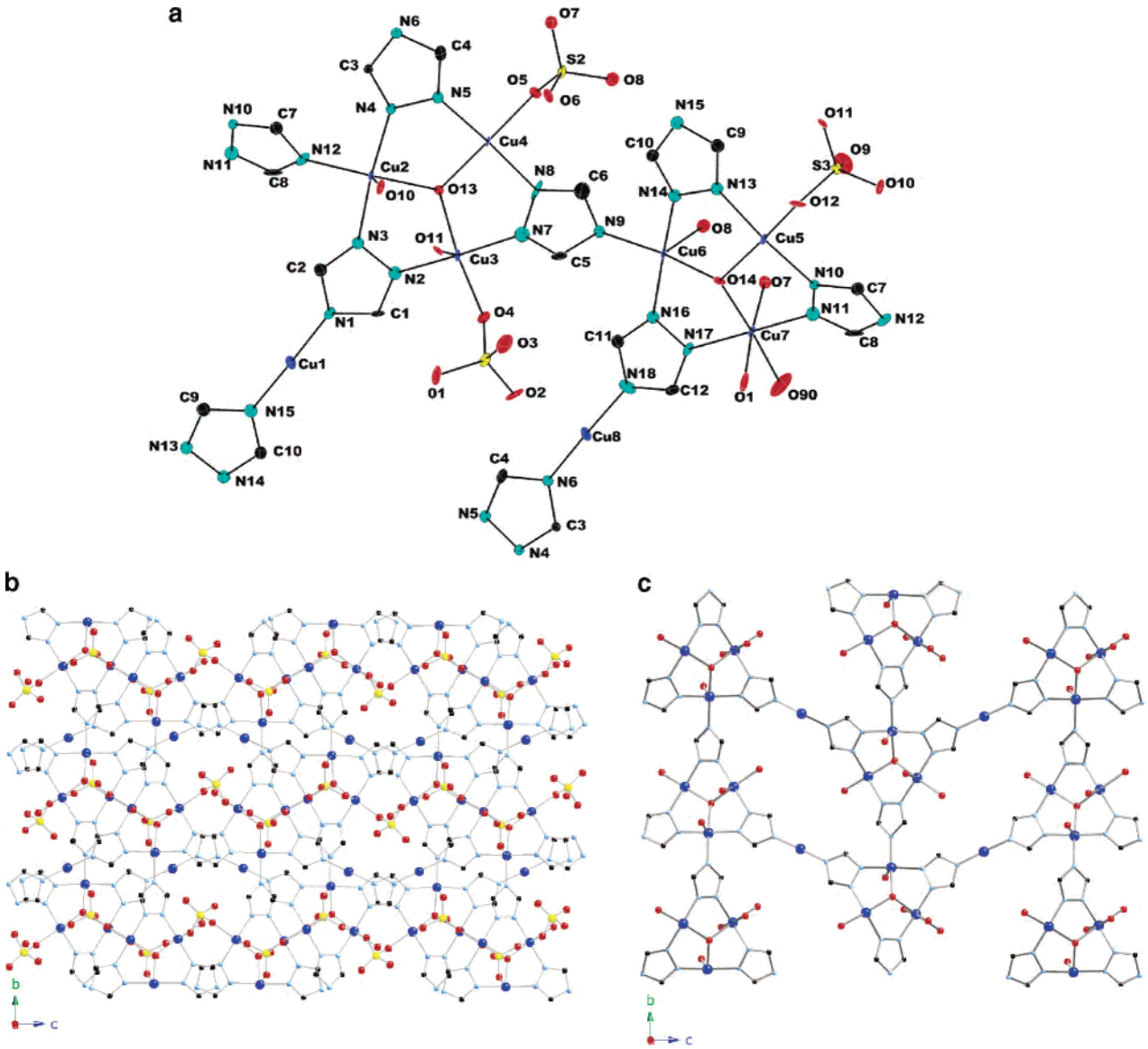

Figure 8. (a) ORTEP view of the structure of **8**, showing the atom-labeling scheme and 50% thermal ellipsoids. (b) Three-dimensional structure of **8** in the *bc* plane. (c) View of the connectivity between $\{Cu_3(trz)_3(\mu^3\text{-}OH)\}^{2+}$ clusters in the *bc* plane.

The spatial expansion of the $\{Cu_4(trz)_3\}_n$ motif is not planar. Alternate triangular units when viewed along the crystallographic *c* axis are rotated by 38.2° with respect to each other to produce the interlocking three-dimensional framework of Figure 9c.

As noted in Table 3, the compounds of this study exhibit a number of close Cu···Cu contacts. While the issue of Cu···Cu bonding in Cu^I continues to be controversial,[44−47] metallophilic bonding has been invoked to rationalize close Cu···Cu distances in a number of compounds,[48,49] including molecular species exhibiting the trinuclear motif of compound **9**. The intratrimer distances of **9** are quite similar to those previously reported for $\{(CF)pzCu\}_3$[44] and $\{(3,4,5\text{-}Me)_3pzCu\}_3$ (pz = pyrazolate),[50] where the short Cu···Cu distances are attributed to the bridging ligands. The intertrimer separations, on the other hand, may reflect true cuprophilicity.

It is noteworthy that the relevant Cu···Cu contacts fall in the 3.00−3.60-Å range with the exceptions of distances of 2.727 Å in **6** and 2.518 Å in $[Cu_3(trz)_2][Cu_2(trz)Cl]Cl\cdot 3H_2O$. Curiously, these two compounds exhibit quite distinct substructures in the construction of their overall architectures. Thus, **6** consists of $\{Cu(trz)\}_n$ chains linked to $\{CuI\}_n$ chains, and the short Cu···Cu interactions occur within the $\{CuI\}_n$ chain. In the case of $[Cu_3(trz)_2][Cu_2(trz)Cl]Cl\cdot 3.H_2O$, there are distinct cationic layers $\{Cu_3(trz)_2\}_n^{n+}$ and neutral $\{Cu_2(trz)Cl\}_n$ chains. The short contact distance occurs between

(44) Dias, H. V. R.; Diyabalanage, H. V. K.; Eldabaja, M. G.; Elbjeirami, O.; Rawashdeh-Omary, M. A.; Omary, M. A. *J. Am. Chem. Soc.* **2005**, *127*, 7489 and references cited therein.
(45) Clerac, R.; Cotton, F. A.; Daniels, L. M.; Gu, J.; Murillo, C. A.; Zhou, H. C. *Inorg. Chem.* **2000**, *39*, 4488.
(46) Carvajal, M. A.; Alvarez, S.; Novoa, J. J. *Chem.—Eur. J.* **2004**, *10*, 2117.
(47) Poblet, J.-M.; Benard, M. *Chem. Commun.* **1998**, *11*, 1179.
(48) Kohn, R. D.; Seifert, G.; Pan, Z.; Mahon, M. F.; Kociok-Kohen, G. *Angew. Chem., Int. Ed.* **2003**, *42*, 793.
(49) Pyykkö, P. *Chem. Rev.* **1997**, *97*, 599.
(50) Ehlert, M. K.; Rettig, S. J.; Storr, A.; Thompson, R. C.; Trotter, J. *Can. J. Chem.* **1992**, *70*, 2161.

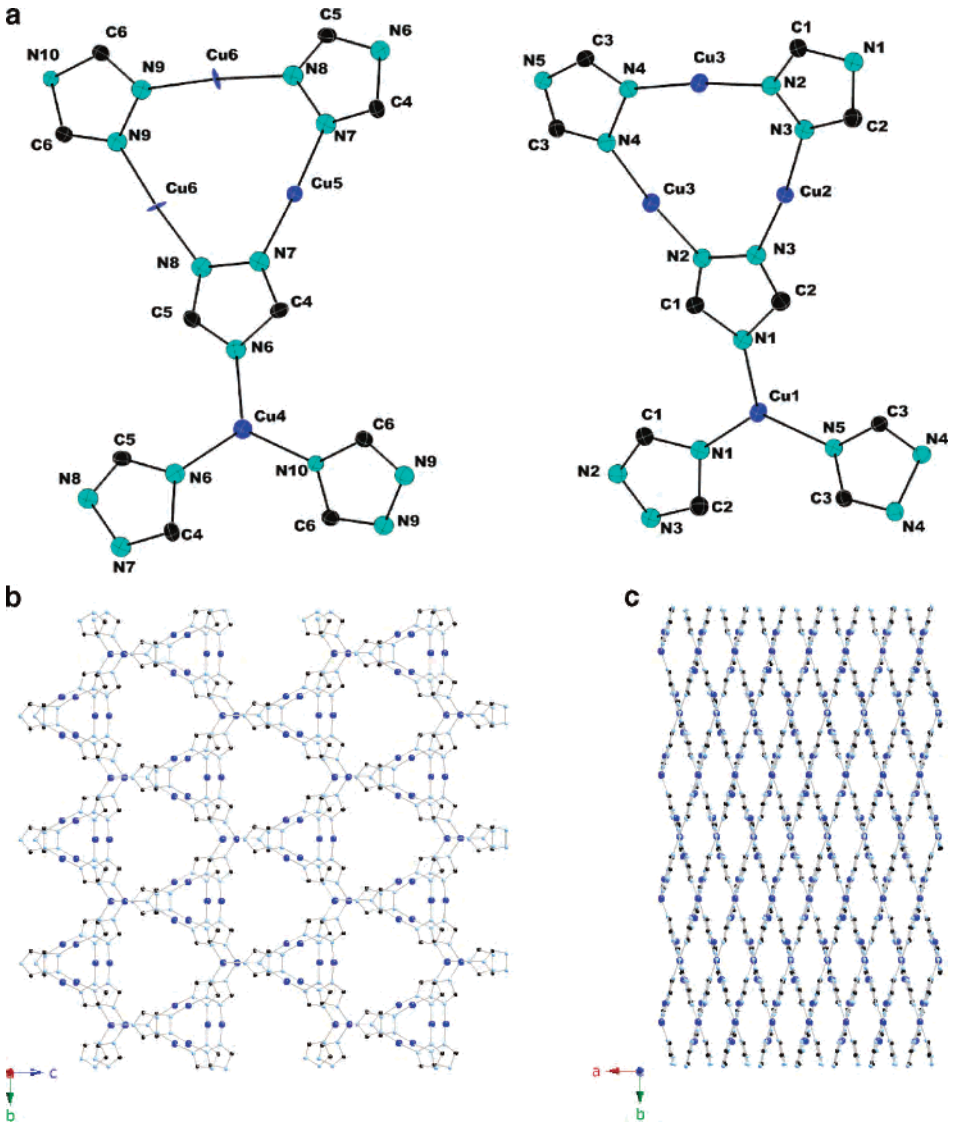

Figure 9. (a) ORTEP view of the structure of **9**·7.5H_2O, showing the atom-labeling scheme and 50% thermal ellipsoids. (b) View of the structure of **9**·7.5H_2O in the *bc* plane. (c) Three-dimensional structure of **9** in the *ab* plane.

Cu sites of the two structural components. While such cuprophilic interactions are weak, it has been argued that their occurrence can profoundly influence the luminescence properties of these materials (vide infra).

While the hydrothermal phases of the Cu/trz/anion family of this study and the previously reported $[Cu_3(trz)_3(OH)_3(H_2O)_4]$·4.5$H_2O$, $[Cu_3(trz)_2][Cu_2(trz)Cl]Cl$·3$H_2O$, and $[Cu_3(trz)_3OH][Cu_2Br_4]$ all exhibit three-dimensional structures, the frameworks are constructed from distinct building blocks and substructures, revealing an unusual structural diversity. As noted in Table 2, the Cu^{I} sites display a full range of coordination modes—linear, trigonal planar with $\{X_3\}$, $\{NX_2\}$, and $\{N_2X\}$ donor sets and tetrahedral with $\{NX_3\}$ and $\{X_4\}$ donor sets—while the Cu^{II} centers exhibit square-planar geometry with $\{N_4\}$ and $\{N_2O_2\}$ donor sets, axially distorted "4 + 1" or square-pyramidal coordination with $\{N_4O\}$, $\{N_3O_2\}$, $\{N_2O_3\}$, and $\{N_2X_3\}$ donor sets, and axially distorted "4 + 2" or octahedral sites with $\{N_2X_4\}$ and $\{N_2O_4\}$ donors.

The absence of a structural system for the Cu/trz/anion family also reflects the rich diversity of copper halide structural chemistry, which provides a variety of oligomeric and polymeric architectures.[51−55] Furthermore, oligomeric copper halide substructures do not appear universally as embedded structural components of these materials. Copper halide chains are structural features of compounds **4**−**7**, while compound **2** exhibits $\{Cu_2Cl_2\}_n^{n+}$ networks and $[Cu_3(trz)_3(OH)][Cu_2Br_4]$ exhibits a three-dimensional $\{CuBr_2\}_n^{n-}$ substructure. In contrast, phases **1** and **3** do not exhibit spatially extended copper halide components. In these cases, spatial expansion is accomplished through the triazolate bridges, as manifested in one-, two-, and three-dimensional $\{Cu_x(trz)_y\}$ substructures. It is noteworthy that materials

(51) Willett, R. D.; Twambley, B. *Inorg. Chem.* **2004**, *43*, 953.
(52) Graham, P. M.; Pike, R. D.; Sabat, M.; Bailey, R. D.; Pennington, W. D. *Inorg. Chem.* **2000**, *39*, 5121.
(53) Place, H.; Scott, B.; Willett, R. D. *Inorg. Chim. Acta* **2001**, *319*, 403.
(54) Place, H.; Scott, B.; Willett, R. D. *Inorg. Chim. Acta* **1998**, *279*, 1.
(55) DeBord, J. R. D.; Lu, Y.-J.; Warren, C. J.; Haushalter, R. C.; Zubieta, J. *Chem. Commun.* **1997**, 1365.

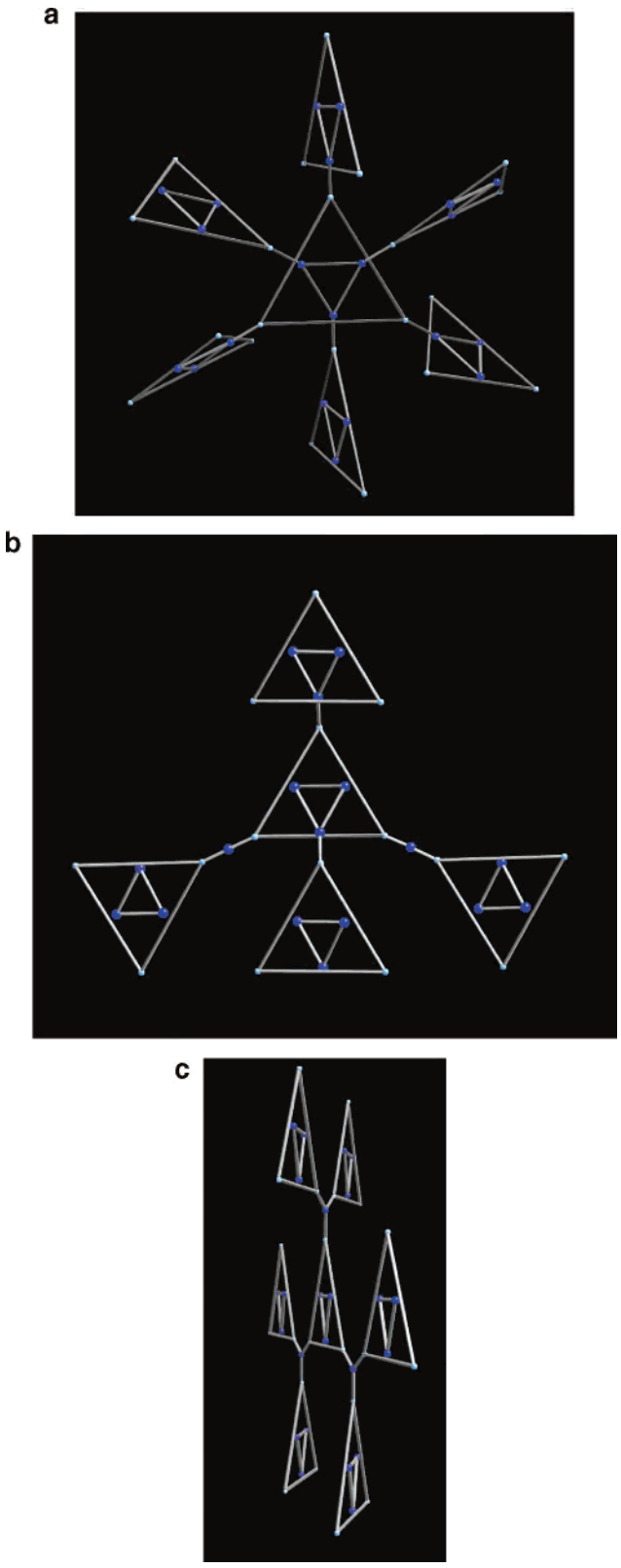

Figure 10. Schematic representations of the linking of trinuclear building blocks of $[Cu_3(trz)_3(OH)_3(H_2O)_4]$, **8**, and **9**.

constructed from copper halide and N-heterocyclic donor bridging ligands and prepared under conventional, nonhydrothermal conditions appear to retain oligomeric and polymeric copper halide substructures.[56]

Table 3. Relevant Cu···Cu Distances (Å) for the Cu^I Materials of This Study, $[Cu_5(trz)_3Cl_2]$ and Related Compounds

compound	Cu···Cu
$[Cu_6(trz)_4Br_2]$ (**3**)	3.149−3.379 (intralayer) 3.154−3.458 (interlayer)
$[Cu_6(trz)_4Br][Cu_4Br_4(OH)]$ (**4**)	3.508 (intralayer) 3.224, 3.424 (interlayer, alternating)
$[Cu_3(trz)I_2]$ (**6**)	3.447 (between substructural chains) 2.717, 3.518 (within $\{CuI\}_n$ chains)
$[Cu_4(trz)_3]OH\cdot 7.5H_2O$ (**9**)	3.502 (exocyclic, interlayer) 3.395−3.481 (intra-trinuclear clusters) 3.502−3.508 (inter-trinuclear clusters)
$[Cu_3(trz)_2][Cu_2(trz)Cl]Cl\cdot 3H_2O$	3.135 (intra-1-D substructure) 3.315−3.356 (intra-2-D substructures) 2.518 (inter-1-D/2-D substructures)
$\{(CF_{-3})pzCu\}_3$	3.214−3.264 (intra-trinuclear clusters) 3.100−3.482 (inter-trinuclear clusters)
$\{(3,4,5\text{-}Me)_3pzCu\}_3$	3.212 (intra-trinuclear clusters) 3.069 (inter-trinuclear clusters)

On the other hand, several metal/trz building units are recurrent themes in the structural chemistry of such compounds.[38,40,57−61] As illustrated in Figure 11, there are a

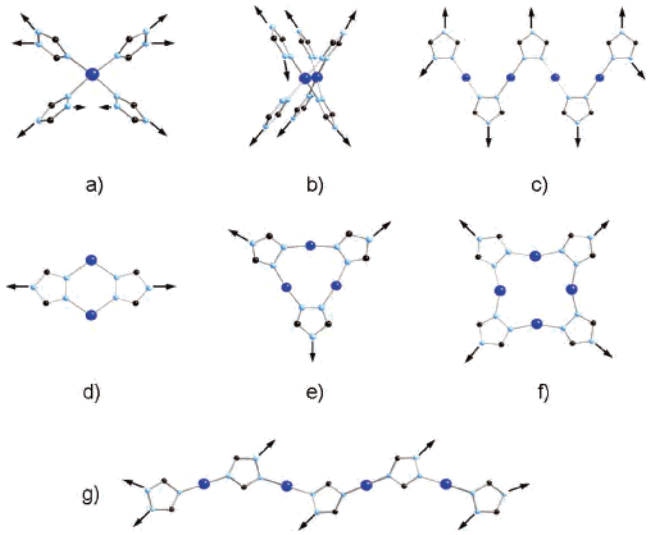

Figure 11. Common building units for the construction of Cu/trz materials.

number of simple binary Cu/1,2,4-trz units that provide cores for the construction of polymeric materials. Thus, compound **1** of this study exploits the expansion of the motif illustrated in Figure 11a, while phase **7** is constructed from the one-dimensional motif of Figure 11b. Similarly, the one-dimensional building units of parts c and g of Figure 11 are embedded in the three-dimensional structures of **2** and **5** and of **3** and **6**, respectively. As noted above, the trinuclear core of Figure 11e is common to the structures of **8**, **9**, and several other Cu/trz's, while the tetranuclear unit of Figure 11b is present in **4**. While the building unit of Figure 11d has been identified in a variety of materials, including [Cu(mtrz)] (mtrz = 3,5-dimethyl-1,2,4-triazolate)[16] and [Cu(ptrz)] (ptrz = 3,5-

(56) Blake, A. J.; Brooks, N. R.; Champness, N. R.; Hanton, L. R.; Hubberstey, P.; Schröder, M. *Pure Appl. Chem.* **1998**, *70*, 2351.
(57) Park, H.; Moureau, D. M.; Parisi, J. B. *Chem. Mater.* **2006**, *18*, 525.
(58) Zhang, J.-P.; Liu, Y.-Y.; Huang, X.-C.; Chen, X.-M. *Dalton Trans.* **2005**, 3681.
(59) Yi, L.; Ding, B.; Zhao, B.; Cheng, P.; Liao, D.-Z.; Yan, S.-P.; Jiang, Z.-H. *Inorg. Chem.* **2004**, *43*, 33.
(60) Kröber, J.; Bkouche-Waksman, I.; Pascard, C.; Thomann, M.; Kahn, O. *Inorg. Chim. Acta* **1995**, *230*, 159.
(61) Zhang, J.-P.; Tong, M.-L.; Chen, X.-M. *Angew. Chem., Int. Ed.* **2002**, *41*, 1029.

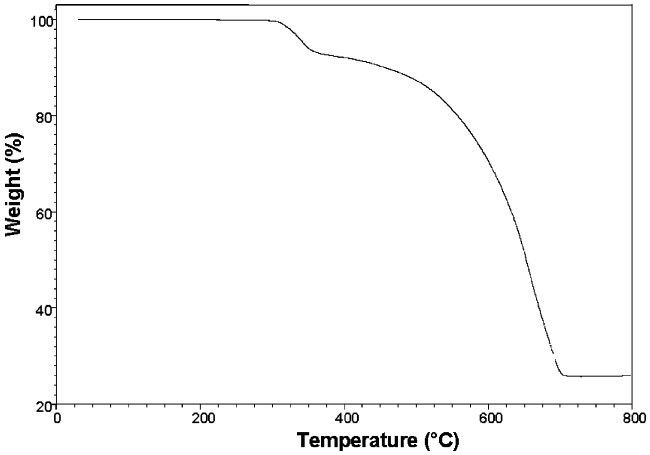

Figure 12. TGA curve for **3**.

dipropyl-1,2,4-triazolate),[57] it does not occur as a subunit of the structures of this study.

The structural chemistry is further complicated by the coordination of water molecules or hydroxide anions. Coordinated water and/or hydroxide is observed only for the Cu^{II} sites of **1**, **8**, $[Cu_3(trz)_3(OH)_3(H_2O)_4]$, and $[Cu_3(trz)_3(OH)][Cu_2Br_4]$. Furthermore, the open framework of the Cu^{I} phase **9** accommodates both solvent water and isolated, charge-balancing hydroxide.

The most significant structural determinant appears to be the identity of the anion X. Consequently, F does not coordinate to the Cu sites but rather provides a charge-balancing anion, while Br and I contribute to different polymeric substructures in **5**−**7** and $[Cu_3(trz)_3(OH)][Cu_2Br_4]$. Incorporation of sulfate in **8** and cyanide in $[Cu_6(CN)_5(trz)]$[40] results in uniquely complex structural prototypes.

Thermogravimetric Analyses (TGA). The compounds **3**−**5**, **8**, **9**, and $[Cu_3(trz)_2][Cu_2(trz)Cl]Cl$ were analyzed by TGA under 20 mL min^{-1} flowing nitrogen while ramping the temperature at a rate of 5° min^{-1} from 25 to 800 °C. The thermal decomposition profiles are generally quite similar to those previously observed for coordination polymers of copper halides with nitrogenous donor ligands.[62,63] As shown in Figure 12 for **3**, there is an initial weight loss of approximately 8% between 330 and 350 °C, corresponding to the loss of one triazolate ligand. This initial weight loss is then followed by a decomposition process accounting for 67% of the mass in the 500−700 °C range. This latter process is associated with the loss of the organic ligand and sublimation of CuBr (68%, theoretical) to leave a residue of Cu.

$$[Cu_6(trz)_4Br_2] \xrightarrow[-trz]{300-350\ ^\circ C} [Cu_6(trz)_3Br_2]$$

$$[Cu_6(trz)_3Br_2] \xrightarrow[-CuBr]{500-700\ ^\circ C} Cu^0$$

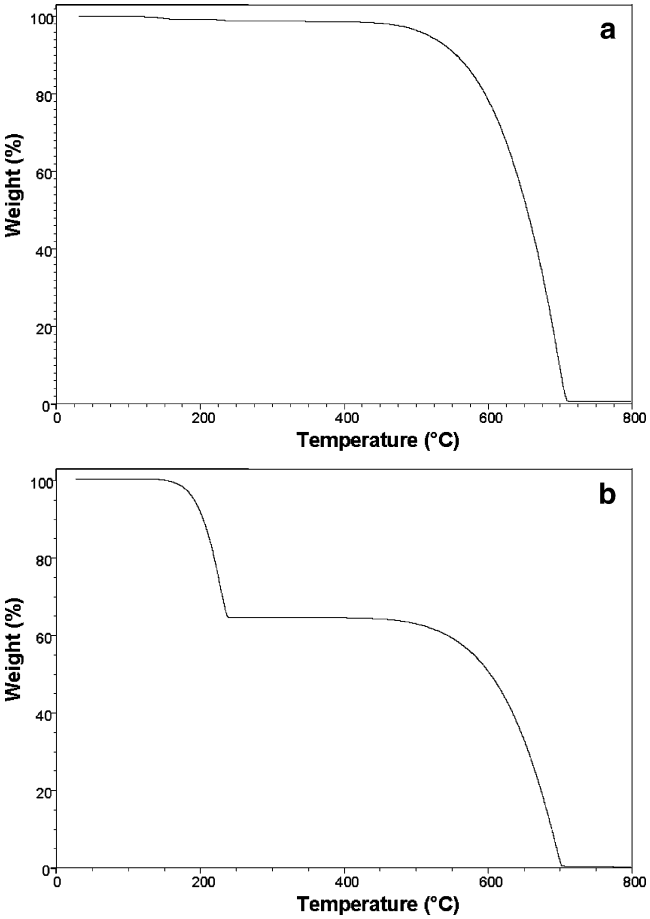

Figure 13. TGA profiles for (a) CuBr and (b) $CuBr_2$.

A comparison of the thermal behavior of **3** with those of $CuBr_2$ and CuBr in Figure 13 illustrates that $CuBr_2$ decomposes by loss of Br_2(g) at ca. 200 °C to produce CuBr, which subsequently sublimes between 560 and 700 °C, with a profile similar to that observed for the second decomposition step of **3**.

The thermodiffraction pattern for compound **3** in the temperature range 25−450 °C is shown in Figure 14. The X-ray profile of **3** persists to 425 °C whereupon a new phase begins to appear. Despite loss of some organic residues between 330 and 350 °C, the thermodiffraction behavior suggests that the structural integrity of the material is retained beyond this temperature. The major phase appearing above 425 °C is CuBr. Upon cooling, the resultant CuBr persists to room temperature. The thermal characteristics of compounds **4** and **5** are similar to those described for **3**. The TGA profiles of both exhibit the loss of ca. one triazolate at 325−350 °C, followed by a second weight loss between 450 and 700 °C associated with combustion of the remaining organic residues and sublimation of CuBr. However, in contrast to the structural stability of the framework of **3**, the thermodiffraction pattern for **4** demonstrates that the initial weight loss results in the collapse of the framework structure of **4** and the appearance of the CuBr phase at 325 °C. Apparently, the framework of **3** is considerably more thermally robust than that of **4**.

(62) Graham, P. M.; Pike, R. D.; Sabat, M.; Bailey, R. D.; Pennington, W. T. *Inorg. Chem.* **2000**, *39*, 5121.
(63) Maeyer, J. T.; Johnson, T. J.; Smith, A. K.; Borne, B. D.; Pike, R. D.; Pennington, W. T.; Krawiec, M.; Rheingold, A. L. *Polyhedron* **2003**, *22*, 419.

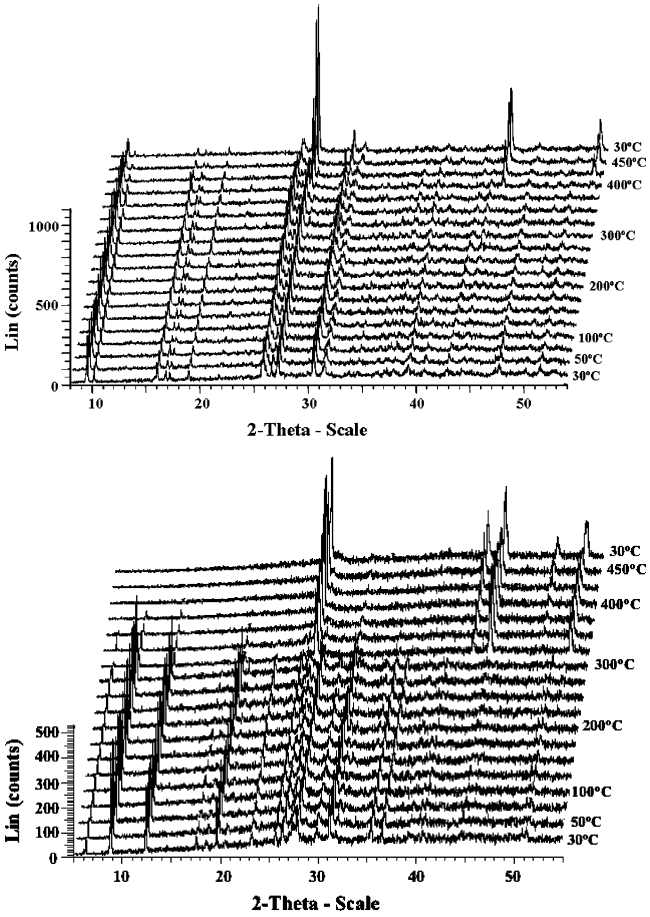

Figure 14. Thermodiffraction pattern for (a) **3** and (b) **4** in the 30−425 °C temperature range.

The thermal characteristics of **8** and **9** are unexceptional for compounds of this class. Compound **8** exhibits a sharp weight loss of ca. 26% at 340 °C, followed by a gradual loss of an additional 31% in the 340−620 °C range. The initial weight loss is in the range associated with partial loss of the triazolate residues, with the remainder of the organic residues, the aqua and hydroxy, and the sulfate lost in the second step (total weight loss obsd, ca. 58%; theory, 59.6%).

Compound **9** exhibits a dehydration process at 80−140 °C, followed by a rapid loss of 16% between 290 and 310 °C (total weight loss obsd, 23%; theory for $7.5H_2O$, 22.1%). These initial weight losses are followed by a continuous weight loss of 35% in the 340−640 °C range, corresponding to the loss of the organic residues. The thermodiffractogram of **9** demonstrates that the structure collapses above 140 °C, suggesting that dehydration is sufficient to destroy the framework in this instance. The product of this dehydration is amorphous.

In contrast to the sulfate and hydroxide phases **8** and **9**, $[Cu_3(trz)_2][Cu_2(trz)Cl]Cl$ exhibits thermal characteristics reminiscent of the bromide phases **3**−**5**. There is an initial weight loss at 320 °C, corresponding to the partial loss of triazolate, followed by a continuous weight loss from 440 to 660 °C associated with the remaining organic residues and sublimation of CuCl.

Magnetic Properties. Several families of organic−inorganic materials, such as metal phosphonates, oxalates, hydroxides, and others,[64−66] exhibit remarkable magnetic properties. The superexchange capacity of the triazolate ligand endows many of its metal complexes with unusual magnetic properties.[21−24]

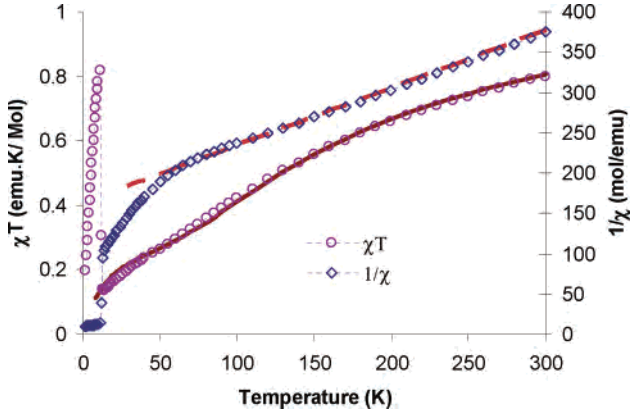

Figure 15. Temperature dependence of χT (○) and of the inverse susceptibility $1/\chi$ (◇) for **1**. The solid line corresponds to the best fit obtained with eq 2 and the dashed line is the fit to the Curie−Weiss law.

Magnetic susceptibility measurements of complexes **1**, **5**, **7**, **8**, and the previously reported $[Cu_3(trz)_3(OH)][Cu_2Br_4]$ were performed on polycrystalline samples of compounds at 1000 Oe over the temperature range 2−300 K.

The value of χT at 300 K is 0.8 emu mol^{-1} K for compound **1** , which is smaller than the expected value for three Cu^{II} ions ($3\chi_{Cu}T = 1.125$ cm^3 mol^{-1} K and $S = {}^1/_2$; Figure 15). The χT value continuously decreases from room temperature and reaches a minimum of 0.13 emu mol^{-1} K at 13 K. Below 13 K, χT increases abruptly to reach a maximum at ∼11 K ($\chi T_{max} = 0.82$ emu mol^{-1} K) and finally decreases again at lower temperatures. The temperature dependence of $1/\chi$ between 300 and 60 K approximates Curie−Weiss behavior with $C = 1.4$ emu mol^{-1} K and $\theta = -230$ K. The negative sign of the Curie−Weiss constant indicates antiferromagnetic interactions between Cu^{II} centers.

To explain the magnetic interaction among Cu ions, the local magnetic pathways must be considered. The connectivity of the material dictates that bonding within the Cu trimers formed by two N−N bridges will dominate the magnetic properties, with much weaker coupling between the trimers through bridging triazolate groups.

A simple isotropic model nicely describes the magnetic behavior above 13 K in terms of one trimeric unit $Cu_A-Cu_B-Cu_A$. The Hamiltonian, $H = -J(S_A \cdot S_B + S_B \cdot S_A)$, describes the interactions of the three $S = {}^1/_2$ Cu centers. On the basis of the molecular structure, the interaction between Cu_A ions has been assumed to be negligible and $J_{A-B} = J_{B-A}$ and $g_A \neq g_B$. This yielded the following expression for the χT:[67,68]

(64) Bellitto, C. *Magnetism: Molecules to Materials*; Miller, J. S., Drillon, M., Eds.; CNR−Instituto di Chimica dei Materiali: Rome, Italy, 2001; pp 425−456.
(65) Pilkington, M.; Decurtins, S. *Perspect. Supramol. Chem.* **2003**, *7*, 275.
(66) Rabiu, P.; Drillon, M.; Awaga, K.; Fujita, W.; Sehine, T. *Magnetism: Molecules to Materials II*; Miller, J. S., Drillon, M., Eds.; CNR−Instituto di Chimica dei Materiali: Rome, Italy, 2001; pp 357−395.
(67) Bacchi, A.; Carcelli, M.; Pelizzi, G.; Solinas, C.; Sorace, L. *Inorg. Chim. Acta* **2006**, *359*, 2275.

$$\chi T = \frac{N\beta^2}{4k} \frac{[(4g_A - g_B)/3]^2 + g_B \exp(J/kT) + 10[(2g_A + g_B)/3]^2 \exp(3J/2kT)}{1 + \exp(J/kT) + 2\exp(3J/2kT)} \quad (1)$$

Because of the magnetic interactions between the individual trimeric magnetic units, eq 1 was corrected using the molecular field approximation (eq 2), where χ is the experimental exchange-coupled magnetic susceptibility, χ_{Cu} is the magnetic susceptibility of the Cu trimer, zJ' is the exchange parameter, and the other symbols have their usual connotations:[69]

$$\chi = \frac{\chi_{Cu}}{1 - (zJ'/Ng^2\beta^2)\chi_{Cu}} \quad (2)$$

The magnetic data were fit to eq 2 in the temperature range 13−300 K with the parameters $J = -130$ cm^{-1}, $g_A = 2.0$, $g_B = 2.2$, and $zJ' = -51$ cm^{-1}, which are in good agreement with values reported for similar compounds.[67]

The observed increase in χT below 13 K corresponds to a weak ferromagnetic ordering at low temperatures due to spin canting of the antiferromagnetically coupled trimer units. The ordering was verified by comparing the zero-field-cooled (ZFC) susceptibility of compound **1** to the data obtained on a field-cooled (FC) sample (Figure 16). The divergence of direct-current ZFC and FC samples reveals the history dependence of the magnetization process. The remnant magnetization conforms to the FC sample, thus excluding any relaxation properties. The decrease in χT below 11 K is a result of saturation at high magnetic field.

Magnetization measurements performed at 1.8 K revealed an abrupt increase of the magnetic moment at low fields with a steady increase to a value of 0.15 μ_B at 70 kOe (Figure 17). No saturation was observed. Hysteresis loops measured at 1.8 K are consistent with a weak ferromagnet for **1** with coercive fields of 210 Oe and remnant magnetization values (M_r) of 0.0095 (Figure 17, inset). The spontaneous magnetization is, therefore, due to a spin canting, with an estimated canting angle of 0.5°. This angle is calculated using the equation $\psi = \tan^{-1}(M_r/M_s)$, where M_r is the remnant magnetization and $M_s = gS$ is the expected saturation magnetization if all of the moments are aligned ferromagnetically.[70,71]

The χT and χ vs T plots per one Cu^{II} ion for **5** are shown in Figure 18. The value of χ_m is 0.0013 emu mol^{-1} at room temperature, increases smoothly to a maximum of 0.0045 emu mol^{-1} at 40 K, and finally decreases to 0.003 emu mol^{-1} at 2 K. The value of χT at 300 K is 0.4 emu mol^{-1} K, which corresponds to one Cu^{II} ion per unit cell ($S = {}^1/_2$ and $g = 2.2$). The decrease of χT upon cooling indicates the presence

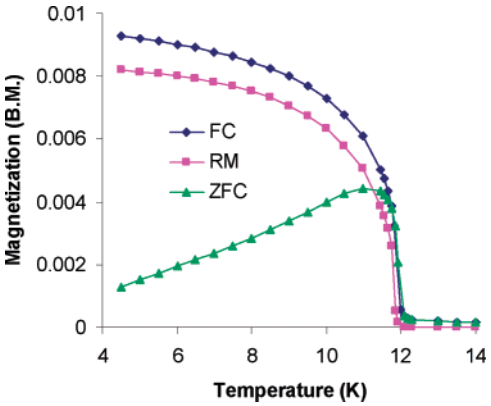

Figure 16. ZFC (△), FC (◇), and remnant (□) magnetization data for **1**, measured at an applied field of $H = 20$ Oe.

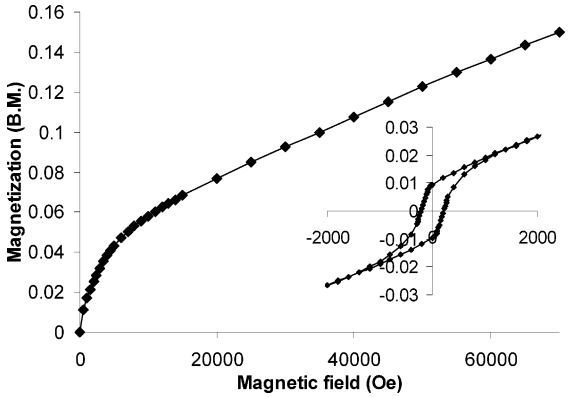

Figure 17. Field-dependent magnetization and hysteresis loop (inset) for **1** measured at 1.8 K.

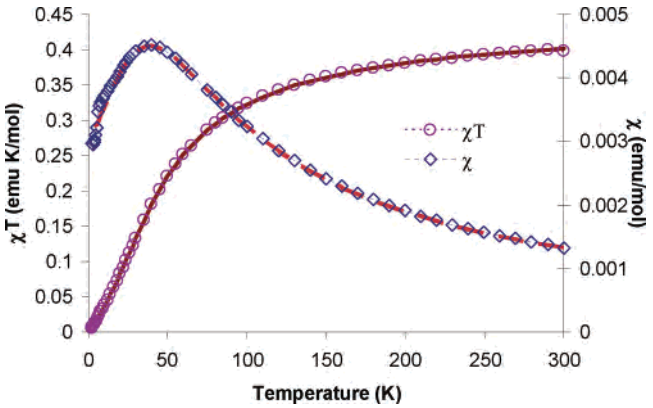

Figure 18. Temperature dependence of χT (○) and χ (◇) for compound **5**. The solid and dashed lines are the best fits to the $S = {}^1/_2$ chain model.

of an antiferromagnetic interaction between Cu^{II} centers. Because well-isolated Cu^{II} chains are the dominant magnetic units in this material, the magnetic data were fitted by the simple one-dimensional chain model[72] (the Hamiltonian is written as $H = -JS_iS_{i-l}$). This model produced a good fit to the experimental data over the whole temperature range. The parameters of the fitting are listed in Table 4.

The χT and χ vs T plots for **7** are similar to those of compound **5** (Figure S10 in the Supporting Information). The plot of χ_m vs T shows a value of 0.001 emu mol^{-1} at room

(68) Kong, D.; Li, Y.; Ouyang, X.; Prosvirin, A. V.; Zhao, H.; Ross, J. R., Jr.; Dunbar, K. D.; Clearfield, A. *Chem. Mater.* **2004**, *16*, 3020.
(69) Kahn, O. *Molecular Magnetism*; VCH: New York, 1993.
(70) Marvilliers, A.; Parsons, S.; Riviere, E.; Audiere, J.-P.; Kurmoo, M.; Mallah, T. *Eur. J. Inorg. Chem.* **2001**, 1287.
(71) Palacio, F.; Andres, M.; Horne, R.; van Duyneveldt, A. J. *J. Magn. Magn. Mater.* **1986**, *54−57*, 1487.
(72) Estes, W. E.; Gavel, D. P.; Hatfield, W. E.; Hodgson, D. J. *Inorg. Chem.* **1978**, *6*, 1415.

Table 4. Fitting Parameters for the Magnetic Susceptibilities for Compounds **1**, **5**, **7**, **8**, and $[Cu_3(trz)_3(OH)][Cu_2Br_4]$

compound	fitting model	J (cm^{-1})	zJ' (cm^{-1})	g	monomeric impurity (%)
1	linear trimer	−130	−51	2,0, 2.2	0
5	1-D chain	−164	0	2.2	0
7	1-D chain	−450	0	2.13	1.2
8	triangle	−204	−38	2.25	0
$[Cu_3(trz)_3(OH)]$-$[Cu_2Br_4]$	triangle	−180	−68	2.2	0

temperature, which increases smoothly to a maximum of 0.0016 emu mol^{-1} at 100 K, then decreases and reaches a minimum of 0.0014 emu mol^{-1} at 10 K, and finally increases to 0.0027 emu mol^{-1} at 2 K. The value of χT at 300 K is 0.31 emu mol^{-1} K, which is lower than the expected value for a spin-only case ($\chi_{Cu}T = 0.374$ emu mol^{-1} K and $S = {}^1/_2$). The decrease in χT from room temperature indicates an antiferromagnetic interaction between Cu^{II} centers. The parameters of the magnetic fitting to the one-dimensional chain model are listed in Table 4.

The unit cell of compound **8**, $[Cu_8(trz)_2(SO_4)_3(OH)_2(H_2O)]$, contains two equilateral Cu^{II} triangles as the dominant magnetic blocks. The value of χT at 300 K is 0.75 emu mol^{-1} K per trimer, which is smaller than the expected value for three Cu^{II} ions ($3\chi_{Cu}T = 1.125$ cm^3 mol^{-1} K and $S = {}^1/_2$; Figure 19). The χT value continuously decreases from room

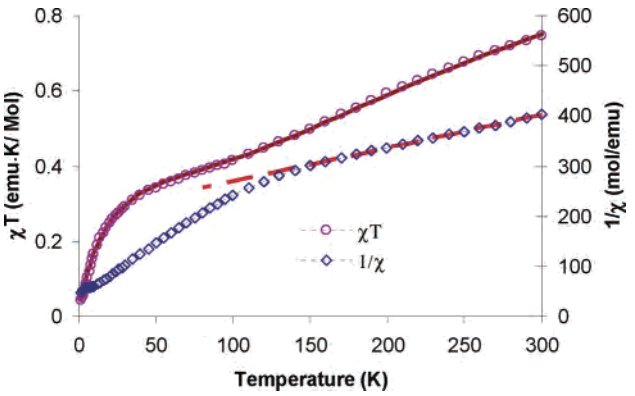

Figure 19. Temperature dependence of χT (○) and of the inverse susceptibility (◇) for **8**. The solid line corresponds to the best fit to eq 2, and the dashed line is the fit to the Curie−Weiss law.

temperature and reaches a minimum of 0.047 emu mol^{-1} K at 2 K. The temperature dependence of $1/\chi$ between 300 and 130 K approximates Curie−Weiss behavior with $C = 1.51$ emu mol^{-1} K and $\theta = -310$ K, which indicates antiferromagnetic interactions between Cu^{II} centers. From the structure of **8** and considering that the three metals are structurally almost equivalent, so that as $J_A = J_B = J_C$ and $g_A = g_B = g_C$, the spin Hamiltonian $H = -J(S_A \cdot S_B + S_B \cdot S_C + S_C \cdot S_A)$ can be used to describe the magnetic interactions.[17,67,68] From this Hamiltonian, the magnetic susceptibility may be described by eq 3. The magnetic data were fit using the

$$\chi T = \frac{N\beta^2 g^2}{4k} \frac{1 + 5\exp(3J/2kT)}{1 + \exp(3J/2kT)} \qquad (3)$$

molecular field approximation (eq 2) over the whole temperature range of 2−300 K with the parameters $J = -204$ cm^{-1}, $g = 2.25$, and $zJ' = -38$ cm^{-1}, in good agreement with those reported for similar compounds.[17,73−75]

Table 5. Summary of Solid-State Photophysical Data for Triazole, **3**, **4**, **6**, **9**·7.5H_2O, and $[Cu_3(trz)_2][Cu_2(trz)Cl]Cl \cdot 3H_2O$

compound	λ_{ex} (298 K) (nm)	λ_{max} (298 K) (nm)	λ_{ex} (77 K) (nm)	λ_{max} (77 K) (nm)	τ/μ_s 298 K	τ/μ_s 77 K	assignment
triazole	318	421	320	423	*a*	8.5	$^3[\pi-\pi^*]$[47]
3	328	534	318	556	63.7	77.3	^{3}[MLCT]
4	291	496	314	518	20.5	30.2	^{3}[MLCT]
6	334	636	322	698	*a*	5.5	^{3}[MLCT]
9	325	612	306	650	65.9	161.8	^{3}[MLCT]
$[Cu_5(trz)_3$-$Cl_2]$	342	664			28.2		^{3}[MLCT]
			330	462		51.4	^{3}[XLCT]

[a] Lifetime too short to measure.

The magnetic properties of $[Cu_3(trz)_3(OH)][Cu_2Br_4]$ are almost identical with those of **8**, as expected because it also contains equilateral Cu^{II} triangles as the dominant magnetic units. The value of χT at 300 K is 0.71 emu mol^{-1} K per trimer, which is smaller than the expected value for three Cu^{II} ions (Figure S11 in the Supporting Information). The χT value continuously decreases from room temperature to 0.013 emu mol^{-1} K at 2 K. The temperature dependence of $1/\chi$ between 300 and 100 K approximates Curie−Weiss behavior with $C = 1.4$ emu mol^{-1} K and $\theta = -300$ K, which indicates antiferromagnetic interactions between Cu^{II} centers. A reasonable fit to eq 3 corrected for intertrimer interactions (eq 2) was obtained. The fitting parameters are again listed in Table 4.

Photoluminescence Properties. The photoluminescence characteristics of the Cu^I species **3**, **4**, **6**, and **9** of this study and of the previously reported $[Cu_3(trz)_2][Cu_2(trz)Cl]Cl \cdot 3H_2O$[39] are summarized in Table 5. The crystals of these Cu^{II} species exhibit bright phosphorescence at room temperature in all cases. In addition, the compounds possess striking luminescence thermochromium. The emissions for **3**, **4**, **6**, and **9** and the room-temperature emissions of $[Cu_3(trz)_2][Cu_2(trz)Cl]Cl \cdot 3H_2O$ are tentatively assigned as originating from ^{3}[MLCT] excited states. This assignment is consistent with the broad and unstructured emission profiles and the long luminescence lifetimes of ca. 6−80 μs,[76,77] as well as comparisons to related Cu^I molecular and solid-state materials.[44,78−80]

The consistent increase in the lifetimes of the excited states upon cooling from room temperature to 77 K may be rationalized as a result of the reduction of the nonradiative decay rate. The luminescence thermochromium varies con-

(73) Ferrer, S.; Haasnoot, J. G.; Reedijk, J.; Muller, E.; Biagini Cingi, M.; Lanfranchi, M.; Manotti Lanfredi, A. M.; Ribas, J. *Inorg. Chem.* **2000**, *39*, 1859.
(74) Angaridis, P. A.; Baran, P.; Boca, R.; Cervantes-Lee, F.; Haase, W.; Mezei, G.; Raptis, R. G.; Werner, R. *Inorg. Chem.* **2002**, *41*, 2219.
(75) Jiang, Y.-B.; Kou, H.-Z.; Wang, R.-J.; Cui, A.-L.; Ribas, J. *Inorg. Chem.* **2005**, *44*, 709.
(76) Ford, P. C.; Cariati, E.; Bourassa, J. *Chem. Rev.* **1999**, *99*, 3625.
(77) Yan, V. W.-W. *Acc. Chem. Res.* **2002**, *35*, 555.
(78) Omary, H. V. K.; Gamage, C. S. P.; Dias, H. V. R. *Inorg. Chem.* **2005**, *44*, 8200 and references cited therein.
(79) Zhang, J.-P.; Lin, Y.-Y.; Huang, X.-C.; Chen, X.-M. *J. Am. Chem. Soc.* **2005**, *127*, 5495.
(80) Wong, W.-Y.; Liu, L.; Shi, J.-X. *Angew. Chem., Int. Ed.* **2003**, *42*, 4064.

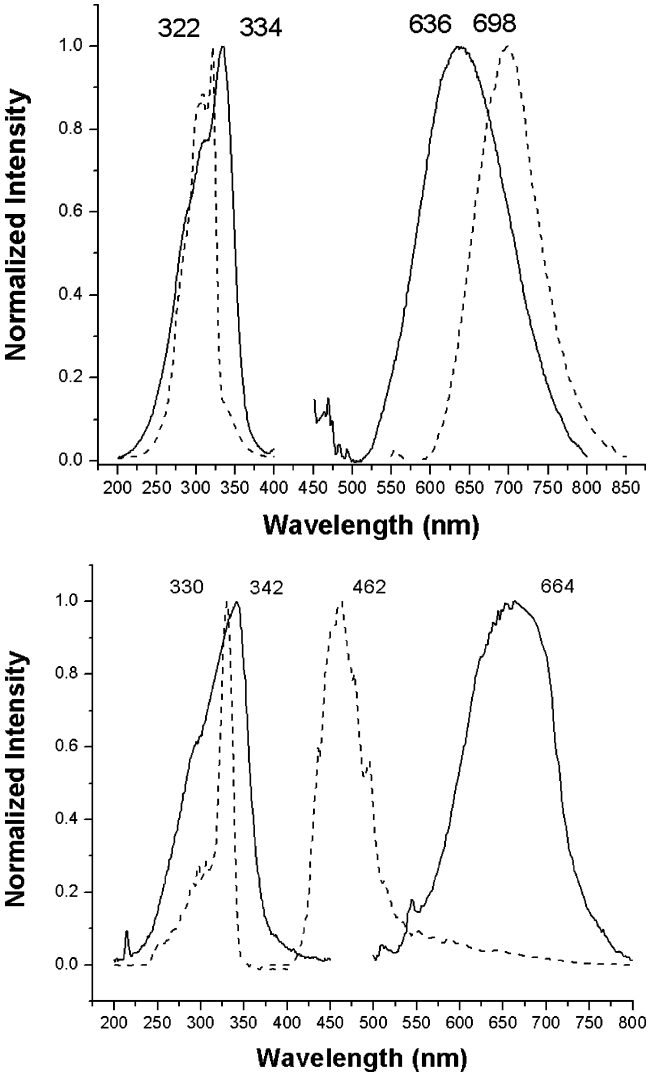

Figure 20. (a) Photoluminescence spectra of **6** at room temperature (solid lines) and 77 K (dashed lines). (b) Photoluminescence spectra of $[Cu_5(trz)_3Cl_2]$ at room temperature (solid lines) and 77 K (dashed lines).

siderably in the series of compounds. This observation reflects the structural difference between the compounds, the different halide constituents, and possibly the range of Cu···Cu distances associated with the structures. Because metal−metal interactions affect the emission properties of Cu^I species, metal-centered ^{3}[MC] or metal−metal "bond" to ligand charge transfer ^{3}[MMLCT] excited states should also be considered.

In this respect, of the compounds of this study, the materials **3**, **4**, and **9** exhibit an average red shift of 27 nm in their emission bands upon cooling from room temperature to 77 K. In contrast, the shift for **6** is 62 nm (Figure 20). It may be significant that **6** is the only member of this set that exhibits a Cu···Cu contact shorter than the 3.00−3.60-Å range.

The most dramatic thermochromic behavior is shown by $[Cu_3(trz)_2][Cu_2(trz)Cl]Cl\cdot 3H_2O$, which at room temperature exhibits excitation and emission spectra similar to those of the other compounds of this study. However, at 77 K, the Stokes' shift of the emission is ca. 100−200 cm^{-1} smaller than those of the other compounds of this study, suggesting a different origin for this band. One possibility is a ^{3}[XLCT], a halide (X) to ligand charge transfer. It is also noteworthy that the structure of $[Cu_3(trz)_2][Cu_2(trz)Cl]Cl\cdot 3H_2O$ is distinct from those of the compounds of this study. In contrast to the exclusively covalent connectivities of **3**, **6**, and **9**, $[Cu_3(trz)_2][Cu_2(trz)Cl]Cl\cdot 3H_2O$ is constructed from independent $\{Cu_3(trz)_2\}_n^{n+}$ networks, $\{Cu_2(trz)Cl\}_n$ chains, and isolated, charge-balancing Cl^- anions. Consequently, as noted previously, the structure exhibits a broad range of Cu···Cu interactions within and between the substructural motifs, including a contact of 2.518 Å between structural subunits. It is noteworthy that the two compounds with the most dramatic shifts in emission bands upon cooling, **6** and $[Cu_3(trz)_2][Cu_2(trz)Cl]Cl\cdot 3H_2O$, also exhibit the most pronounced cuprophilic interactions. The photoluminescence properties of these materials and of the related Zn^{II} and Cd^{II} species will be discussed in detail in a forthcoming contribution.

Conclusions

Hydrothermal chemistry has been exploited in the preparation of a series of three-dimensional phases of the Cu/trz/anion family where the anion (X) is F^-, Cl^-, Br^-, I^-, OH^-, or SO_4^{2-}. The rich structural chemistry of these phases reflects a number of structural determinants, including the identity of the anionic component and the reaction conditions of stoichiometry, temperature, and pH. Although embedded polymeric copper halide substructures are characteristic of copper halide/organonitrogen ligand phases isolated under more conventional, nonhydrothermal conditions, the materials of this study do not uniformly possess such extended substructures. While **2**, **4**−**7**, and $[Cu_3(trz)_3(OH)][Cu_2Br_4]$ exhibit $\{Cu_xX_y\}_n$ substructures, **1**, **3**, **8**, $\mathbf{9}\cdot 7.5H_2O$, and $[Cu_3(trz)_3(OH)_3(H_2O)_4]\cdot 4.5H_2O$ are constructed from polymeric $\{Cu_x(trz)_y\}_n$ components.

In common with other families of hydrothermally synthesized materials, identical starting materials can provide different phases, depending on the reaction conditions. Thus, we have identified two copper chloride phases (**2** and $[Cu_3(trz)_2][Cu_2(trz)Cl]Cl\cdot 3H_2O$), four copper bromide phases (**3**−**5** and $[Cu_3(trz)_3OH][Cu_2Br_4]$), and two copper iodide compounds (**6** and **7**).

The magnetic properties of the Cu^{II}-containing phases reflect the structural diversity of the system. Compound **1** exhibits simple isotropic behavior above 13 K, while weak ferromagnetic ordering is observed below this temperature. The temperature-dependent susceptibilities of compounds **5** and **7** conform to the one-dimensional chain model, while **8** and $[Cu_3(trz)_3(OH)][Cu_2Br_4]$ exhibit magnetic properties consistent with three Cu^{II} sites antiferromagnetically coupled in a trinuclear array.

The Cu^I materials **3**, **4**, **6**, **9**, and $[Cu_3(trz)_2][Cu_2(trz)Cl]Cl\cdot 3H_2O$ exhibit luminescence thermochromism. All exhibit broad and unstructured emission profiles, large Stokes' shifts, and long luminescence lifetimes consistent with phosphorescence originating from ^{3}[MLCT] excited states. The most dramatic thermochromic behavior is shown by **6** and $[Cu_3(trz)_2][Cu_2(trz)Cl]Cl\cdot 3H_2O$. Curiously, these are also the only compounds of this study that exhibit significant cuprophilic

interactions. The photoluminescence properties of these compounds and of the related Zn^{II} and Cd^{II} compounds are under investigation.

Acknowledgment. This work was funded by a grant from the National Science Foundation (Grant CHE-0604527).

Supporting Information Available: Crystallographic files in CIF format for compounds **1**−**9** and Figures S1−S9, showing the atom-labeling schemes and 50% thermal ellipsoids for compounds **1**−**9**, respectively, Figure S10, showing the temperature dependence of the χT product and χ for **7**, Figure S11, showing the temperature dependence for χT and the inverse susceptibility for $[Cu_3(trz)_3OH][Cu_2Br_4]$, Figures S12−S16, showing TGA profiles for **4**, **5**, **8**, **9**, and $[Cu_3(trz)_2][Cu_2(trz)Cl]Cl\cdot 3H_2O$, respectively, Figure S17, illustrating the thermodiffraction profile of **9**, and Figures S18−S30, showing the excitation and emission spectra and emission literature measurements for **3**, **4**, **6**, **9**, and $[Cu_3(trz)_2][Cu_2(trz)Cl]Cl$. This material is available free of charge via the Internet at http://pubs.acs.org.

IC061102E